NASA

National Aeronautics and
Space Administration

NASA CR-165412

BOUNDARY LAYER THERMAL STRESSES IN ANGLE-PLY COMPOSITE LAMINATES

Final Report - Part I

by

S.S. Wang and I. Choi

Department of Theoretical and Applied Mechanics
UNIVERSITY OF ILLINOIS
at Urbana-Champaign

prepared for

NATIONAL AERONAUTICS AND SPACE ADMINISTRATION

NASA Lewis Research Center
Grant NSG 3044

1. Report No.	2. Government Accession No.	3. Recipient's Catalog No.
NASA CR-165412		

4. Title and Subtitle	5. Report Date
Boundary Layer Thermal Stresses in Angle-Ply Composite Laminates	February, 1981
	6. Performing Organization Code
7. Author(s)	8. Performing Organization Report No.
S. S. Wang and I. Choi	
	10. Work Unit No.
9. Performing Organization Name and Address	
University of Illinois Urbana, IL 61801	11. Contract or Grant No. NSG 3044
	13. Type of Report and Period Covered Final Report - Part I
12. Sponsoring Agency Name and Address	
National Aeronautics and Space Administration Washington, DC 20546	14. Sponsoring Agency Code

15. Supplementary Notes

Project Manager: C. C. Chamis
Structures & Mechanical Technologies Division
NASA Lewis Research Center, 21000 Brookpark Road, Mail Stop 49-6
Cleveland, OH 44135

16. Abstract

Thermal boundary-layer stresses (near free edges) and displacements are determined by a unique method developed under this grant. This method consists of an eigenfunction expansion technique and the establishment of an appropriate particular solution. Current solutions in the region away from the singular domain (free edge) are found to be excellent agreement with existing approximate numerical results. As the edge is approached, the singular term controls the near field behavior of the boundary layer. Results are presented for cases of various angle-ply graphite/epoxy laminates with $(\theta/-\theta/-\theta/\theta)$ configurations. These results show high interlaminar (through-the-thickness) stresses. Thermal boundary-layer thicknesses of different composite systems are determined by examining the strain energy density distribution in composites. It is shown that the boundary-layer thickness depends on the degree of anisotropy of each individual lamina, thermomechanical properties of each ply, and the relative thickness of adjacent layers. Also, the interlaminar thermal stresses are compressive with increasing temperature. The corresponding residual stresses are tensile and may enhance interply delaminations.

17. Key Words (Suggested by Author(s))	18. Distribution Statement
Stress-analysis, eigen function, boundary layer, free edge singularity, fiber composites, anisotropy	Unclassified, unlimited.

19. Security Classif. (of this report)	20. Security Classif. (of this page)	21. No. of Pages	22. Price*
Unclassified	Unclassified		

* For sale by the National Technical Information Service, Springfield, Virginia 22161

TABLE OF CONTENTS

FOREWORD

This report describes a portion of the results obtained on NASA Grant NSG 3044. This work was done under subcontract to the University of Illinois, Urbana, with Prof. S.S. Wang as the Principal Investigator. The prime grantee was the Massachusetts Institute of Technology, with Prof. F.J. McGarry as the Principal Investigator and Dr. J.F. Mandell as a major participant. The NASA - LeRC Project Manager was Dr. C.C. Chamis.

Efforts in this project are primarily directed towards the development of finite element analyses for the study of flaw growth and fracture of fiber composites. The analysis of such problems using three-dimensional analyses may be limited by the presence of very localized, high stress gradients as occur at free edges. The work described in this report is a theoretical investigation of such effects resulting from thermal or hygroscopic loading. The results given here are for thermal effects, but the same treatment also applies to hygroscopic effects, differing only by the expansion coefficient used. Analogous results to those given here, but for hygroscopic loading, may be found in the following papers:

(1) S.S. Wang and I. Choi, AIAA paper 80-0713-CP, 21st Proceedings of AIAA/ASME/ASCE/AHS Structures, Structural Dynamics and Materials Conf., Seattle, WA, 1980; also to appear in AIAA Journal, November, 1982.

(2) S.S. Wang and I. Choi, in Developments in Composite Materials and Structures, J.R. Vinson, ed., ASME, p. 315 (1980).

ABSTRACT

Thermal stresses near geometric boundaries of fiber-reinforced composite laminates play an important role in controlling complex failure modes and ultimate performance of composite materials in severe thermal environment. This paper presents an investigation of boundary-layer thermal stress singularity and distributions in composite laminates. Based on the theory of anisotropic thermoelasticity, a system of coupled governing partial differential equations is obtained. Edge boundary conditions and interface continuity conditions lead to a transcendental characteristic equation for determining thermal stress singularity at the laminate boundary. Complete thermal boundary-layer stress and displacement solutions are obtained by an eigenfunction expansion method in conjunction with a boundary collocation procedure. The thermoelasticity solution in the region away from the singular domain is found in excellent agreement with existing approximate numerical results. As the edge is approached, the singular terms control the near-field behavior of thermal boundary-layer stresses. Results are presented for the cases of various angle-ply graphite-epoxy laminates with $[\theta/-\theta/-\theta/\theta]$ fiber orientations. Thermal boundary-layer thickness is defined by considering strain energy density distribution along ply interface. The thermal boundary-layer thickness is shown to depend on the anisotropy of individual lamina, ply thermomechanical properties, and relative thickness of adjacent layers.

1. INTRODUCTION

The response of a composite laminate near its geometric boundaries subjected to severe thermal and other environmental loading has attracted much attention recently, since failure of composite materials is frequently initiated at the boundaries. The thermal stress field in the vicinity of the laminate boundaries, which may be primarily responsible for strength degradation and failure of composites, has been investigated by several researchers using different approximate methods [1-4]. Approximate solutions for the thermal boundary-layer problem have revealed several unusual features. Interlaminar stresses near a traction-free boundary of a composite laminate subjected to a uniform temperature change have been found to be very high and inherently three-dimensional. It has also been reported that the high thermal stress is confined within a localized region of several laminar thicknesses from the edge and that in the boundary-layer region they cannot be assessed accurately by the classical lamination theory [5,6]. The behavior of this highly stressed boundary-layer region is of great importance in controlling complex failure modes and ultimate performance of the composites. Understanding the fundamental nature of boundary-layer thermal stresses is essential to the failure analysis, design, and processing optimization of composite materials.

While all previous numerical approximate solutions indicated an unbounded trend of boundary-layer thermal stresses and postulated possible existence of a stress singularity at the edge, the search for the order or strength of the stress singularity has been unsuccessful. No information concerning the exact order of the boundary-layer stress singularity has been reported yet, to the authors' knowledge. The apparent difficulty may result from the complicated nature of the problem such as the thermomechanical anisotropy of each individual

fiber-reinforced lamina, the geometric discontinuity, and the abrupt change of material properties through the laminate thickness direction. Since the thermal boundary-layer effect is localized in nature, it is necessary to determine the exact order of the laminate edge stress singularity so that complex thermal response in the vicinity of laminate boundaries can be studied more accurately. This paper presents a rigorous theoretical study of thermal boundary-layer stress singularity and distributions in composite laminates subjected to uniform thermal loading.

2. FORMULATION

2.1 *Basic Equations*

Consider a general composite laminate composed of fiber-reinforced plies subjected to mechanical and thermal loading, as shown in Fig. 1. Denote the constitutive equation of each individual ply by the Duhamel-Neumann form of generalized Hooke's law in contracted notation as

$$\varepsilon_i = S_{ij}\,\sigma_j + \alpha_i\,\Delta T, \qquad (i,j = 1,2,3,\ldots.6), \tag{1}$$

where the repeated subscript indicates summation; S_{ij} is the compliance tensor; α_i, the thermal expansion coefficient, and ΔT, the change of temperature. The engineering strains, ε_i, in Eq. 1 are defined in a Cartesian coordinate system by

$$\varepsilon_1 = \varepsilon_x = \frac{\partial u}{\partial x}, \qquad \varepsilon_2 = \varepsilon_y = \frac{\partial v}{\partial y}, \qquad \varepsilon_3 = \varepsilon_z = \frac{\partial w}{\partial z},$$

$$\varepsilon_4 = 2\varepsilon_{yz} = \frac{\partial w}{\partial y} + \frac{\partial v}{\partial z}, \qquad \varepsilon_5 = 2\varepsilon_{xz} = \frac{\partial w}{\partial x} + \frac{\partial u}{\partial z}, \qquad \varepsilon_6 = 2\varepsilon_{xy} = \frac{\partial u}{\partial y} + \frac{\partial v}{\partial x}, \tag{2}$$

where u, v and w are displacement components. The stresses, σ_i, are defined in an analogous manner.

The composite laminate considered here has a finite width and is subjected to a uniform axial extension, e, along the z-axis and a uniform temperature change, ΔT. The composite is assumed to be sufficiently long that, in the region far from the end, the end effect is neglected by virtue of Saint Venant's principle. Consequently, stresses in the laminate are independent of the z coordinate. The special case where e vanishes identically corresponds to the well known generalized plane deformation [7]. Under these assumptions, equations of equilibrium without body force read

$$\frac{\partial \sigma_x}{\partial x} + \frac{\partial \tau_{xy}}{\partial y} = 0, \tag{3a}$$

$$\frac{\partial \tau_{xy}}{\partial x} + \frac{\partial \sigma_y}{\partial y} = 0, \tag{3b}$$

$$\frac{\partial \tau_{xz}}{\partial x} + \frac{\partial \tau_{yz}}{\partial y} = 0. \tag{3c}$$

Integrating Eq. 1 with the aid of Eq. 2, one can obtain u, v and w as

$$u = -\frac{z^2}{2}\frac{\partial D}{\partial x} + (S_{5j}\,\sigma_j + \alpha_5\,\Delta T - \frac{\partial W_o}{\partial x})\,z + U_o(x,y), \tag{4a}$$

$$v = -\frac{z^2}{2}\frac{\partial D}{\partial y} + (S_{4j}\,\sigma_j + \alpha_4\,\Delta T - \frac{\partial W_o}{\partial y})\,z + V_o(x,y), \tag{4b}$$

$$w = D\,z + W_o(x,y), \tag{4c}$$

where

$$D = S_{3j}\,\sigma_j + \alpha_3\,\Delta T, \tag{5}$$

and U_o, V_o and W_o are arbitrary functions of x and y only.

Following the procedure in [7], it can be shown after some mathematical manipulation that general expressions for the displacements and the stress component σ_z have the following forms:

$$u = -\frac{1}{2}A_1\,S_{33}\,z^2 - A_4\,yz + U(x,y) + \omega_2\,z - \omega_3\,y + u_o, \tag{6a}$$

$$v = -\frac{1}{2}A_2\,S_{33}\,z^2 + A_4\,xz + V(x,y) + \omega_3\,x - \omega_1\,z + v_o, \tag{6b}$$

$$w = (A_1\,x + A_2\,y + A_3)S_{33}\,z + W(x,y) + \omega_1\,y - \omega_2\,x + w_o, \tag{6c}$$

$$\sigma_z = A_1\,x + A_2\,y + A_3 - (S_{3j}\,\sigma_j + \alpha_3\,\Delta T)/S_{33}, \quad (j = 1,2,4,5,6). \tag{6d}$$

The unknown functions, U, V and W, depend on x and y only, and can be shown easily to obey the following relationships:

$$\frac{\partial U}{\partial x} = \tilde{S}_{1j}\,\sigma_j + S_{13}(A_1\,x + A_2\,y + A_3) + \tilde{\alpha}_1\,\Delta T, \tag{7a}$$

$$\frac{\partial V}{\partial y} = \tilde{S}_{2j}\,\sigma_j + S_{23}(A_1\,x + A_2\,y + A_3) + \tilde{\alpha}_2\,\Delta T, \tag{7b}$$

$$\frac{\partial W}{\partial x} = \tilde{S}_{5j}\,\sigma_j + S_{53}(A_1\,x + A_2\,y + A_3) + A_4\,y + \tilde{\alpha}_5\,\Delta T, \tag{7c}$$

$$\frac{\partial W}{\partial y} = \tilde{S}_{4j}\,\sigma_j + S_{43}(A_1\,x + A_2\,y + A_3) - A_4\,x + \tilde{\alpha}_4\,\Delta T, \tag{7d}$$

$$\frac{\partial U}{\partial y} + \frac{\partial V}{\partial x} = \tilde{S}_{6j}\,\sigma_j + S_{63}(A_1\,x + A_2\,y + A_3) + \tilde{\alpha}_6\,\Delta T, \tag{7e}$$

$$(j = 1,2,4,5,6).$$

where

$$\tilde{S}_{ij} = S_{ij} - S_{i3}\,S_{j3}/S_{33}, \tag{8a}$$

$$\tilde{\alpha}_i = \alpha_i - \alpha_3\,S_{i3}/S_{33} \qquad (i,j = 1,2,4,5,6). \tag{8b}$$

It is obvious that the constants, u_o, v_o, w_o and $\omega_i (i = 1,2,3)$, in Eqs. 6a-6d characterize the rigid body translation and rotation of the solid. A_1 and A_2 represent the bending of the laminate in the x-z and y-z planes, respectively. A_3 characterizes the uniform axial extension of the composite laminate, and A_4, the relative angle of rotation about the z-axis.

2.2 *Governing Partial Differential Equations, and Boundary and End Conditions*

Introducing Lekhnitskii's stress functions, F and Ψ, such that

$$\sigma_x = \frac{\partial^2 F}{\partial y^2}, \qquad \sigma_y = \frac{\partial^2 F}{\partial x^2}, \qquad \tau_{xy} = -\frac{\partial^2 F}{\partial x\,\partial y},$$

$$\tau_{xz} = \frac{\partial \Psi}{\partial y}, \qquad \tau_{yz} = -\frac{\partial \Psi}{\partial x}, \tag{9a-e}$$

one can show that the equations of equilibrium are satisfied identically. Eliminating U and V from Eqs. 7a, 7b and 7e, and W from Eqs. 7c and 7d, one obtains the following system of governing partial differential equations:

$$\begin{cases} L_3\, F + L_2\, \Psi = -\, 2A_4 + A_1\, S_{34} - A_2\, S_{35} - H_1\, \Delta T, & (10a) \\ L_4\, F + L_3\, \Psi = -\, H_2\, \Delta T, & (10b) \end{cases}$$

where L_2, L_3, L_4, H_1, and H_2 are linear differential operators defined as

$$L_2 = \tilde{S}_{44}\, \frac{\partial^2}{\partial x^2} - 2\tilde{S}_{45}\, \frac{\partial^2}{\partial x\, \partial y} + \tilde{S}_{55}\, \frac{\partial^2}{\partial y^2}, \tag{11a}$$

$$L_3 = -\, \tilde{S}_{24}\, \frac{\partial^3}{\partial x^3} + (\tilde{S}_{25} + \tilde{S}_{46}) \frac{\partial^3}{\partial x^2\, \partial y} - (\tilde{S}_{14} + \tilde{S}_{56}) \frac{\partial^3}{\partial x\, \partial y^2} + \tilde{S}_{15}\, \frac{\partial^3}{\partial y^3}, \tag{11b}$$

$$L_4 = \tilde{S}_{22}\, \frac{\partial^4}{\partial x^4} - 2\tilde{S}_{26}\, \frac{\partial^4}{\partial x^3\, \partial y} + (2\tilde{S}_{12} + \tilde{S}_{66}) \frac{\partial^4}{\partial x^2\, \partial y^2} - 2\tilde{S}_{16}\, \frac{\partial^4}{\partial x\, \partial y^3} + \tilde{S}_{11}\, \frac{\partial^4}{\partial y^4}, \tag{11c}$$

and

$$H_1 = -\, \tilde{\alpha}_4\, \frac{\partial}{\partial x} + \tilde{\alpha}_5\, \frac{\partial}{\partial y}, \tag{11d}$$

$$H_2 = \tilde{\alpha}_2\, \frac{\partial^2}{\partial x^2} - \tilde{\alpha}_6\, \frac{\partial^2}{\partial x\, \partial y} + \tilde{\alpha}_1\, \frac{\partial^2}{\partial y^2}. \tag{11e}$$

Now consider boundary conditions on the lateral surfaces and at the ends of the laminate strip. Assuming that the lateral surfaces are free from surface tractions, one may have the following conditions:

$$\sigma_x\, n_x + \tau_{xy}\, n_y = 0, \tag{12a}$$

$$\tau_{xy}\, n_x + \sigma_y\, n_y = 0, \tag{12b}$$

and

$$\tau_{xz}\, n_x + \tau_{yz}\, n_y = 0, \tag{12c}$$

where n_x and n_y denote the directional cosines of the outward unit normal on ∂B as shown in Fig. 2. The conditions at the ends of the composite laminate may be obtained from the statically equivalent loading as

$$\iint_B \tau_{xz}\, dx\, dy = 0 \tag{13a}$$

$$\iint_B \tau_{yz}\, dx\, dy = 0, \tag{13b}$$

$$\iint_B \sigma_z\, dx\, dy = P_z, \tag{13c}$$

$$\iint_B \sigma_z\, y\, dx\, dy = M_x, \tag{13d}$$

$$\iint_B \sigma_z\, x\, dx\, dy = M_y, \tag{13e}$$

$$\iint_B (\tau_{yz}\, x - \tau_{xz}\, y)\, dx\, dy = M_t, \tag{13f}$$

at $z = \pm L$, where P_z, M_x, M_y, M_t are the applied axial force, bending moments, and twisting moment, respectively.

2.3 *Interface Continuity Conditions*

Consider a portion of the laminate composed of two different fiber-reinforced laminae, as shown in Fig. 2. Stress functions of Eqs. 9a and 9b must be defined for each ply. Assuming that the plies are perfectly bonded along the interface ∂B_I, one can immediately establish the continuity conditions of the stress and displacement along the interface between the kth and (k+1)th plies as the following:

$$\sigma_x^{(k)}\, n_x^{(k)} + \tau_{xy}^{(k)}\, n_y^{(k)} = -\sigma_x^{(k+1)}\, n_x^{(k+1)} - \tau_{xy}^{(k+1)}\, n_y^{(k+1)}, \tag{14a}$$

$$\tau_{xy}^{(k)}\, n_x^{(k)} + \sigma_y^{(k)}\, n_y^{(k)} = -\tau_{xy}^{(k+1)}\, n_x^{(k+1)} - \sigma_y^{(k+1)}\, n_y^{(k+1)}, \tag{14b}$$

$$\tau_{xz}^{(k)}\, n_x^{(k)} + \tau_{yz}^{(k)}\, n_y^{(k)} = -\tau_{xz}^{(k+1)}\, n_x^{(k+1)} - \tau_{yz}^{(k+1)}\, n_y^{(k+1)}, \tag{14c}$$

and

$$u^{(k)} = u^{(k+1)}, \tag{15a}$$

$$v^{(k)} = v^{(k+1)}, \tag{15b}$$

$$w^{(k)} = w^{(k+1)}. \tag{15c}$$

By using divergence theorem, it can be readily seen that Eqs. 13a and 13b are satisfied identically by virtue of 3c, 12c and 14c. Substituting the displacements, Eqs. 6a-c, into the above continuity conditions, Eqs. 15a-c, one finds that the unknown constants for two adjacent layers in Eq. 6 are related by

$$u_o^{(k)} = u_o^{(k+1)}, \qquad v_o^{(k)} = v_o^{(k+1)}, \qquad w_o^{(k)} = w_o^{(k+1)}, \tag{16a-c}$$

$$\omega_1^{(k)} = \omega_1^{(k+1)}, \qquad \omega_2^{(k)} = \omega_2^{(k+1)}, \tag{16d-e}$$

$$U^{(k)} - \omega_3^{(k)} y = U^{(k+1)} - \omega_3^{(k+1)} y, \quad V^{(k)} + \omega_3^{(k)} x = V^{(k+1)} + \omega_3^{(k+1)} x, \quad W^{(k)} = W^{(k+1)}, \tag{16f-h}$$

and

$$A_i^{(k)} \; S_{33}^{(k)} = A_i^{(k+1)} \; S_{33}^{(k+1)}, \qquad (i = 1,2,3) \tag{16i}$$

$$A_4^{(k)} = A_4^{(k+1)}. \tag{16j}$$

3. METHOD OF SOLUTION

The complex governing differential equations and boundary conditions formulated in the previous section may be simplified considerably as appropriate loading conditions and geometric symmetry are taken into consideration. For simplicity and without loss of generality, the following geometric and environmental conditions are introduced for the present thermal boundary-layer stress problem:

(a) the temperature change ΔT is constant and uniformly distributed throughout the laminate, and there is no external mechanical loading applied;

(b) the interface is a straight line and meets the traction-free edge of the composite laminate by a right angle.

Under these assumptions the governing differential Eqs.10a and 10b may be simplified as

$$L_3 F + L_2 \Psi = -2A_4 + A_1 S_{34} - A_2 S_{35}, \tag{17a}$$

$$L_4 F + L_3 \Psi = 0, \tag{17b}$$

with boundary and end conditions,

$$\sigma_x = \tau_{xy} = \tau_{xz} = 0, \qquad \text{on } x = 0, \tag{18a-c}$$

$$\iint_B \sigma_z \, dx \, dy = \iint_B \sigma_z \, x \, dx \, dy = \iint_B \sigma_z \, y \, dx \, dy = 0, \qquad \text{on B,} \tag{19a}$$

$$\iint_B (\tau_{yz} \, x - \tau_{xz} y) dx \, dy = 0, \qquad \text{on B.} \tag{19b}$$

The interface continuity conditions of tractions and displacements may be expressed as the following:

$$\sigma_y^{(k)} = \sigma_y^{(k+1)}, \qquad \tau_{xy}^{(k)} = \tau_{xy}^{(k+1)}, \qquad \tau_{yz}^{(k)} = \tau_{yz}^{(k+1)}, \tag{20a}$$

$$U^{(k)} = U^{(k+1)}, \qquad V^{(k)} + \omega_3^{(k)} x = V^{(k+1)} + \omega_3^{(k+1)} x, \qquad W^{(k)} = W^{(k+1)}, \tag{20b}$$

along $y = 0$, as the original of the coordinate system is moved to the free edge.

3.1 *Homogeneous Solution*

The simplified governing differential equations, Eqs. 17a and 17b, are coupled, linear partial differential equations with constant coefficients related to the anisotropic thermomechanical elastic constants of each composite lamina. The general solution consists of a homogeneous solution and a particular solution depending on geometric, loading, and boundary conditions of the problem under consideration. Lehknitskii has shown [7] that the homogeneous solution of the above mentioned system of governing partial differential equations has the general form

$$F(x,y) = \sum_{k=1}^{6} F_k(x + \mu_k y), \tag{21a}$$

$$\Psi(x,y) = \sum_{k=1}^{6} \eta_k F_k'(x + \mu_k y), \tag{21b}$$

where the prime (') in Eq. 21b denotes differentiation of the function $F_k(x + \mu_k y)$ with respect to its argument, and the coefficients μ_k are the roots of the following algebraic characteristic equation:

$$\ell_4(\mu)\, \ell_2(\mu) - \ell_3^2(\mu) = 0, \tag{22a}$$

and

$$\eta_k = - \ell_3(\mu_k)/\ell_2(\mu_k) = - \ell_4(\mu_k)/\ell_3(\mu_k), \tag{22b}$$

with

$$\ell_2(\mu) = \tilde{S}_{55}\, \mu^2 - 2\tilde{S}_{45}\, \mu + \tilde{S}_{44}, \tag{22c}$$

$$\ell_3(\mu) = \tilde{S}_{15}\,\mu^3 - (\tilde{S}_{14} + \tilde{S}_{56})\mu^2 + (\tilde{S}_{25} + \tilde{S}_{46})\,\mu - \tilde{S}_{24}, \tag{22d}$$

$$\ell_4(\mu) = \tilde{S}_{11}\,\mu^4 - 2\tilde{S}_{16}\,\mu^3 + (2\tilde{S}_{12} + \tilde{S}_{66})\,\mu^2 - 2\tilde{S}_{26}\,\mu + \tilde{S}_{22}. \tag{22e}$$

It has been shown [7] that Eq. 22a cannot have a real root. Thus the roots μ_k appear as complex conjugates, and F_k are analytic functions of the complex variables $Z_k = x + \mu_k y$. Substituting the expressions of $F(x,y)$ and $\Psi(x,y)$ in Eqs. 21a and 21b into Eqs. 9a-e, the homogeneous components of the stress σ_i may be expressed in terms of $F_k(Z_k)$ as

$$\sigma_x^{(h)} = \sum_{k=1}^{6} \mu_k^2\, F_k''(Z_k), \tag{23a}$$

$$\sigma_y^{(h)} = \sum_{k=1}^{6} F_k''(Z_k), \tag{23b}$$

$$\tau_{yz}^{(h)} = -\sum_{k=1}^{6} \eta_k\, F_k''(Z_k), \tag{23c}$$

$$\tau_{xz}^{(h)} = \sum_{k=1}^{6} \mu_k\, \eta_k\, F_k''(Z_k), \tag{23d}$$

$$\tau_{xy}^{(h)} = -\sum_{k=1}^{6} \mu_k\, F_k''(Z_k). \tag{23e}$$

The expressions for displacement components may be obtained directly from Eqs. 7, 10 and 23 with omission of terms which are to be included in the particular solution. Hence, one has

$$u^{(h)} = \sum_{k=1}^{6} p_k\, F_k'(Z_k), \tag{24a}$$

$$v^{(h)} = \sum_{k=1}^{6} q_k\, F_k'(Z_k), \tag{24b}$$

and

$$w^{(h)} = \sum_{k=1}^{6} t_k \, F_k'(Z_k), \tag{24c}$$

where

$$p_k = \tilde{S}_{11} \, \mu_k^2 + \tilde{S}_{12} - \tilde{S}_{14} \, \eta_k + \tilde{S}_{15} \, \eta_k \, \mu_k - \tilde{S}_{16} \, \mu_k, \tag{24d}$$

$$q_k = \tilde{S}_{12} \, \mu_k + \tilde{S}_{22}/\mu_k - \tilde{S}_{24} \, \eta_k/\mu_k + \tilde{S}_{25} \, \eta_k - \tilde{S}_{26}, \tag{24e}$$

$$t_k = \tilde{S}_{14} \, \mu_k + \tilde{S}_{24}/\mu_k - \tilde{S}_{44} \, \eta_k/\mu_k + \tilde{S}_{45} \, \eta_k - \tilde{S}_{46}. \tag{24f}$$

We now choose the form of $F_k(Z_k)$ as

$$F_k(Z_k) = C_k \, Z_k^{\delta+2}/[(\delta+1)(\delta+2)], \tag{25}$$

where C_k and δ are arbitrary complex constants to be determined later. Substituting Eq. 25 into Eqs. 23 and 24 gives

$$\sigma_x^{(h)} = \sum_{k=1}^{3} [C_k \, \mu_k^2 \, Z_k^{\delta} + C_{k+3} \, \overline{\mu}_k^2 \, \overline{Z}_k^{\delta}], \tag{26a}$$

$$\sigma_y^{(h)} = \sum_{k=1}^{3} [C_k \, Z_k^{\delta} + C_{k+3} \, \overline{Z}_k^{\delta}], \tag{26b}$$

$$\tau_{yz}^{(h)} = - \sum_{k=1}^{3} [C_k \, \eta_k \, Z_k^{\delta} + C_{k+3} \, \overline{\eta}_k \, \overline{Z}_k^{\delta}], \tag{26c}$$

$$\tau_{xz}^{(h)} = \sum_{k=1}^{3} [C_k \, \eta_k \, \mu_k \, Z_k^{\delta} + C_{k+3} \, \overline{\eta}_k \, \overline{\mu}_k \, \overline{Z}_k^{\delta}], \tag{26d}$$

$$\tau_{xy}^{(h)} = - \sum_{k=1}^{3} [C_k \, \mu_k \, Z_k^{\delta} + C_{k+3} \, \overline{\mu}_k \, \overline{Z}_k^{\delta}], \tag{26e}$$

and

$$u^{(h)} = \sum_{k=1}^{3} [C_k \, p_k \, Z_k^{\delta+1} + C_{k+3} \, \overline{p}_k \, \overline{Z}_k^{\delta+1}]/(\delta+1), \tag{27a}$$

$$v^{(h)} = \sum_{k=1}^{3} [C_k\ q_k\ z_k^{\delta+1} + C_{k+3}\ \bar{q}_k\ \bar{z}_k^{\delta+1}]/(\delta+1), \tag{27b}$$

$$w^{(h)} = \sum_{k=1}^{3} [C_k\ t_k\ z_k^{\delta+1} + C_{k+3}\ \bar{t}_k\ \bar{z}_k^{\delta+1}]/(\delta+1), \tag{27c}$$

where the overbar denotes the complex conjugate of the associated variable.

The homogeneous solutions for the stress and displacement shown in Eqs. 26 and 27 are required to satisfy homogeneous boundary conditions and interface continuity conditions, i.e., Eqs. 18 and 20. This leads to a standard eigenvalue problem, which results in a complicated transcendental equation for determining the value of δ. By taking the complex conjugate of Eqs. 26 and 27, it is readily seen that δ_m always appear as pairs of complex conjugates. Thus the stresses and displacements can be made real by superposing the conjugate solutions. It is noted that a similar method of extracting the real function for an isotropic material case was discussed by Theocaris [8] who assumed the stress function including both δ and $\bar{\delta}$ in the formulation. It is also noted that, due to positive definiteness of strain energy of an elastic body, the value of δ_m bounded by $-1 < \mathrm{Re}[\delta_m] < 0$ characterizes the order of singularity of the boundary-layer stress field in the composite laminate. It has been found in a related paper [9] that there is only one real δ_m which meets this condition in the singular boundary-layer stress problem. Detailed information on the edge-stress singularity has been given in Reference 9.

After the eigenvalues, δ_m, are determined, the stress and displacement may be expressed in terms of the resulting eigenfunctions, f_{im} and g_{jm}, as

$$\sigma_i^{(h)} = \sum_m d_m\ f_{im}(x,y;\ \delta_m) \qquad (i = 1,2,4,5,6), \tag{28a}$$

$$u_j^{(h)} = \sum_m d_m \, g_{jm}(x,y;\, \delta_m), \qquad (j = 1,2,3), \tag{28b}$$

where the unknowns d_m are real, and f_{im} and g_{jm} denote known eigenfunctions corresponding to the m-th eigenvalue δ_m.

3.2 *Particular Solution*

The particular solution for the problem may be sought in the form of polynomials as

$$F^{(p)}(x,y) = a_1 x^3 + a_2 x^2 y + a_3 xy^2 + a_4 y^3 + a_5 x^2 + a_6 xy + a_7 y^2, \tag{29a}$$

$$\Psi^{(p)}(x,y) = a_8 x^2 + a_9 xy + a_{10} y^2 + a_{11} x + a_{12} y, \tag{29b}$$

where a_i are arbitrary constants to be determined. It is seen that Eq. 17b is satisfied identically and that Eq. 17a provides the following relation for each ply:

$$\begin{aligned} &-6\tilde{S}_{24}\, a_1 + 2(\tilde{S}_{25} + \tilde{S}_{46})a_2 - 2(\tilde{S}_{14} + \tilde{S}_{56})a_3 \\ &\quad + 6\tilde{S}_{15}\, a_4 + 2\tilde{S}_{44}\, a_8 - 2\tilde{S}_{45}\, a_9 + 2\tilde{S}_{55}\, a_{10} \\ &\quad = -2A_4 + A_1\, S_{34} - A_2\, S_{35}. \end{aligned} \tag{30}$$

Substituting Eqs. 29a and 29b into Eqs. 7 and 9 gives

$$\sigma_x^{(p)} = 2a_3 x + 6a_4 y + 2a_7, \tag{31a}$$

$$\sigma_y^{(p)} = 6a_1 x + 2a_2 y + 2a_5, \tag{31b}$$

$$\tau_{yz}^{(p)} = -2a_8 x - a_9 y - a_{11}, \tag{31c}$$

$$\tau_{xz}^{(p)} = a_9 x + 2a_{10} y + a_{12}, \tag{31d}$$

$$\tau_{xy}^{(p)} = -2a_2 x - 2a_3 y - a_6, \tag{31e}$$

$$\frac{\partial U^{(p)}}{\partial x} = E_{11}\, x + E_{12}\, y + E_{13}, \tag{32a}$$

$$\frac{\partial V^{(p)}}{\partial y} = E_{21}\, x + E_{22}\, y + E_{23}, \tag{32b}$$

$$\frac{\partial W^{(p)}}{\partial y} = (E_{41} - A_4)\, x + E_{42}\, y + E_{43}, \tag{32c}$$

$$\frac{\partial W^{(p)}}{\partial x} = E_{51}\, x + (E_{52} + A_4)\, y + E_{53}, \tag{32d}$$

$$\frac{\partial U^{(p)}}{\partial y} + \frac{\partial V^{(p)}}{\partial x} = E_{61}\, x + E_{62}\, y + E_{63}, \tag{32e}$$

where

$$E_{j1} = 2\tilde{S}_{j1}\, a_3 + 6\tilde{S}_{j2}\, a_1 - 2\tilde{S}_{j4}\, a_8 + \tilde{S}_{j5}\, a_9 - 2\tilde{S}_{j6}\, a_2 + S_{j3}\, A_1, \tag{33a}$$

$$E_{j2} = 6\tilde{S}_{j1}\, a_4 + 2\tilde{S}_{j2}\, a_2 - \tilde{S}_{j4}\, a_9 + 2\tilde{S}_{j5}\, a_{10} - 2\tilde{S}_{j6}\, a_3 + S_{j3}\, A_2, \tag{33b}$$

$$E_{j3} = 2\tilde{S}_{j1}\, a_7 + 2\tilde{S}_{j2}\, a_5 - \tilde{S}_{j4}\, a_{11} + \tilde{S}_{j5}\, a_{12} - \tilde{S}_{j6}\, a_6 + S_{j3}\, A_3 + \tilde{\alpha}_j\, \Delta T. \tag{33c}$$

Integrating Eqs. 32a-e with the aid of Eq. 30, one can obtain

$$U^{(p)} = \frac{1}{2} E_{11}\, x^2 + E_{12}\, xy + E_{13}\, x + \frac{1}{2}(E_{62} - E_{21})\, y^2 + \frac{1}{2} E_{63}\, y, \tag{34a}$$

$$V^{(p)} = E_{21}\, xy + \frac{1}{2} E_{22}\, y^2 + E_{23}\, y + \frac{1}{2}(E_{61} - E_{12})\, x^2 + \frac{1}{2} E_{63}\, x, \tag{34b}$$

$$W^{(p)} = \frac{1}{2} E_{51}\, x^2 + (E_{52} + A_4)\, xy + E_{53}\, x + \frac{1}{2} E_{42}\, y^2 + E_{43}\, y. \tag{34c}$$

Thus the particular solution for the displacement can be written as

$$u^{(p)} = -\frac{1}{2} A_1\, S_{33}\, z^2 - A_4\, yz + U^{(p)}(x,y) + \omega_2\, z - \omega_3\, y + u_o, \tag{35a}$$

$$v^{(p)} = -\frac{1}{2} A_2\, S_{33}\, z^2 + A_4\, xz + V^{(p)}(x,y) + \omega_3\, x - \omega_1\, z + v_o, \tag{35b}$$

$$w^{(p)} = (A_1\, x + A_2\, y + A_3)\, S_{33}\, z + W^{(p)}(x,y) + \omega_1\, y - \omega_2\, x + w_o. \tag{35c}$$

Equations 31 and 35 are required to satisfy the boundary conditions, Eqs. 18a-c, and the interface continuity conditions, Eqs. 20a-b of the current problem. This leads to the establishment of the following relations

$$a_3^{(m)} = a_4^{(m)} = a_6^{(m)} = a_7^{(m)} = a_{10}^{(m)} = a_{12}^{(m)} = 0, \quad (m = k, k+1) \tag{36a}$$

$$a_1^{(k)} = a_1^{(k+1)}, \; a_2^{(k)} = a_2^{(k+1)}, \; a_5^{(k)} = a_5^{(k+1)},$$

$$a_8^{(k)} = a_8^{(k+1)}, \; a_{11}^{(k)} = a_{11}^{(k+1)}, \tag{36b-f}$$

$$E_{11}^{(k)} = E_{11}^{(k+1)}, \; E_{13}^{(k)} = E_{13}^{(k+1)}, \; E_{61}^{(k)} - E_{12}^{(k)} = E_{61}^{(k+1)} - E_{12}^{(k+1)} \tag{36g-i}$$

$$\frac{1}{2} E_{63}^{(k)} + \omega_3^{(k)} = \frac{1}{2} E_{63}^{(k+1)} + \omega_3^{(k+1)}, \; E_{51}^{(k)} = E_{51}^{(k+1)}, \; E_{53}^{(k)} = E_{53}^{(k+1)}. \tag{36j-l}$$

By examining Eqs. 16, 30 and 36, it is observed that there are 44 unknowns (including the unknown rigid-body translations and rotations) related by 34 linear algebraic equations. Solving these equations, there remain ten unknowns (for example, $A_i^{(k)}$, u_o, v_o, w_o and $\omega_i^{(k)}$), which may be determined by Eqs. 19a-b and the boundary conditions other than those on the traction-free edges.

3.3 *Complete Solution*

Now the complete solution for the thermal boundary-layer stress problem can be written as

$$\sigma_i = \sigma_i^{(h)} + \sigma_i^{(p)} \qquad (i = 1,2,4,5,6) , \tag{37a}$$

$$u_j = u_j^{(h)} + u_j^{(p)} \qquad (j = 1,2,3) , \tag{37b}$$

where $\sigma_i^{(h)}$, $u_j^{(h)}$ and $\sigma_i^{(p)}$, $u_j^{(p)}$ are given by Eqs. 28a-b and Eqs. 31, 35, respectively. The solution for the stress, Eq. 37a, satisfies identically the boundary conditions, Eqs. 12a-c, of the free-edge surface ∂B_F. Along ∂B_s ($\partial B_s = \partial B - \partial B_F$), residual stresses appear due to the particular

solution being posed in the previous section. The residual stress can be counterbalanced by the homogeneous solution; thus, on ∂B_s, one obtains

$$\sigma_x^{(h)} n_x + \tau_{xy}^{(h)} n_y = - \sigma_x^{(p)} n_x - \tau_{xy}^{(p)} n_y, \tag{38a}$$

$$\tau_{xy}^{(h)} n_x + \sigma_y^{(h)} n_y = - \tau_{xy}^{(p)} n_x - \sigma_y^{(p)} n_y, \tag{38b}$$

$$\tau_{xz}^{(h)} n_x + \tau_{yz}^{(h)} n_y = - \tau_{xz}^{(p)} n_x - \tau_{yz}^{(p)} n_y. \tag{38c}$$

Without orthogonality among eigenfunctions, Eqs. 38a-c may be satisfied numerically in a least square sense through a boundary collocation method by truncating the eigenfunction series. It is noted that the particular solution is coupled with the homogeneous one through the end conditions, Eqs. 19a-b. Thus by matching Eqs. 38a-c with the aid of Eqs. 19a-b, one can determine all the unknowns explicitly. To this end, the expressions for σ_z may be obtained from Eqs. 6d and 37a as

$$\sigma_z^{(h)} = - S_{3j} \sigma_j^{(h)} / S_{33} \qquad (j=1,2,4,5,6), \tag{39a}$$

$$\sigma_z^{(p)} = A_1 x + A_2 y + A_3 - (S_{3j} \sigma_j^{(p)} + \alpha_3 \Delta T)/S_{33}. \tag{39b}$$

Complete expressions for the displacement field can be written explicitly in a similar manner.

4. NUMERICAL EXAMPLES AND DISCUSSION

For illustration, symmetric angle-ply composite laminates with $[\pm\theta]_s$ orientations are studied. Thermal loading in the form of a uniformly distributed temperature change is considered. The particular laminate configuration and fiber orientation are chosen because approximate numerical solutions for this problem are available in the literature for comparison. Each individual lamina is assumed to be high-modulus graphite-epoxy with the following elastic constants: $E_{11} = E_{22} = 2.1 \times 10^6$ (psi), $E_{33} = 20 \times 10^6$ (psi), $G_{12} = G_{13} = G_{23} = 0.85 \times 10^6$ (psi), $\nu_{12} = \nu_{13} = \nu_{23} = 0.21$, $\alpha_1 = \alpha_2 = 16 \times 10^{-6}$ (/°F), $\alpha_3 = 0.2 \times 10^{-6}$ (/°F), where the subscripts, 1, 2 and 3, refer to transverse, thickness, and longitudinal directions of the individual ply, respectively. The $\tilde{S}_{ij}$ and $\tilde{\alpha}_i$ are evaluated by using these material constants, and the following relationships can be established readily:

$$\tilde{S}^{(\beta)}_{4j} = 0 \quad (j=1,2,3,5,6); \qquad \tilde{S}^{(\beta)}_{6i} = 0 \quad (i=1,2,3,5;\ \beta=1,2);$$

$$\tilde{S}^{(1)}_{ij}=\tilde{S}^{(2)}_{ij} \quad (i,j \le 3); \quad \tilde{S}^{(1)}_{jj}=\tilde{S}^{(2)}_{jj} \quad (j=4,5,6); \quad \tilde{S}^{(1)}_{ij}=-\tilde{S}^{(2)}_{ij} \quad (i,j \ge 4 \text{ and } i \ne j);$$

$$\tilde{\alpha}^{(1)}_{j}=\tilde{\alpha}^{(2)}_{j} \quad (j=1,2); \quad \tilde{\alpha}^{(\beta)}_{4}=\tilde{\alpha}^{(\beta)}_{6}= 0 \ (\beta=1,2); \quad \tilde{\alpha}^{(1)}_{3}=\tilde{\alpha}^{(2)}_{3}; \quad \tilde{\alpha}^{(1)}_{5}=-\tilde{\alpha}^{(2)}_{5}. \tag{40}$$

4.1 *Symmetry Conditions and Further Simplications*

The geometric and lamination symmetry conditions lead to the following relationships:

$$U(x,y) = U(x,-y), \quad V(x,y) = -V(x,-y), \quad W(x,y) = W(x,-y), \tag{41a-c}$$

$$U(x,y) = -U(-x,y), \quad V(x,y) = V(-x,y), \quad W(x,y) = -W(-x,y). \tag{42a-c}$$

Equations 41a-c and 42a-c may be written in equivalent forms as

$$U_{,y}(0,y) = V_{,x}(0,y) = W_{,y}(0,y) = 0, \tag{43}$$

$$U_{,y}(x,0) = V_{,x}(x,0) = W_{,y}(x,0) = 0. \tag{44}$$

The relations provided by Eqs. 7 and 40 and the symmetry conditions given in Eqs. 41 and 42 suggest that

$$A_i^{(1)} = A_i^{(2)} = 0 \qquad (i=1,2,4), \tag{45}$$

and that σ_x, σ_y, σ_z and τ_{xz} are symmetric with respect to the x and y axes and τ_{xy} and τ_{yz} are antisymmetric with respect to the x and y axes. Thus, only $A_3^{(\beta)}$ remains to be determined and only one-quarter of the laminate needs to be considered.

By using Eqs. 40a and 40b, one can easily show that

$$a_5^{(1)} = a_5^{(2)} = -\frac{1}{2}\left[\frac{S_{53}^{(1)}}{\tilde{S}_{52}^{(1)}} A_3^{(1)} + \frac{\tilde{\alpha}_5^{(1)}}{\tilde{S}_{52}^{(1)}} \Delta T\right], \tag{46}$$

$$\omega_3^{(1)} = \omega_3^{(2)}, \tag{47}$$

$$A_3^{(1)} = A_3^{(2)}, \tag{48}$$

and all other unknowns vanish. Thus, the particular solution takes the following forms:

$$\sigma_x^{(p)\beta} = 0, \tag{49a}$$

$$\sigma_y^{(p)\beta} = -\frac{S_{53}^{(1)}}{\tilde{S}_{52}^{(1)}} A_3^{(1)} - \frac{\tilde{\alpha}_5^{(1)}}{\tilde{S}_{52}^{(1)}} \Delta T, \tag{49b}$$

$$\tau_{yz}^{(p)\beta} = \tau_{xz}^{(p)\beta} = \tau_{xy}^{(p)\beta} = 0, \tag{49c}$$

in both layers ($\beta = 1,2$). The displacements may be shown to have the expressions,

$$U^{(p)\beta} = \left[\left[S_{13}^{(1)} - \frac{S_{53}^{(1)}\,\tilde{S}_{12}^{(1)}}{\tilde{S}_{52}^{(1)}}\right] A_3^{(1)} + \left[\tilde{\alpha}_1^{(1)} - \frac{\tilde{S}_{12}^{(1)}}{\tilde{S}_{52}^{(1)}} \tilde{\alpha}_5^{(1)}\right] \Delta T\right] x, \tag{50a}$$

$$V^{(p)\beta} = \left[\left[S_{23}^{(1)} - \frac{S_{53}^{(1)}\,\tilde{S}_{22}^{(1)}}{\tilde{S}_{52}^{(1)}}\right] A_3^{(1)} + \left[\tilde{\alpha}_2^{(1)} - \frac{\tilde{S}_{22}^{(1)}}{\tilde{S}_{52}^{(1)}} \alpha_5^{(1)}\right] \Delta T\right] y, \tag{50b}$$

and

$$W^{(p)\beta} = 0. \tag{50c}$$

Inserting Eqs. 49a-c into Eq. 39b, one can obtain the stress component $\sigma_z^{(p)\beta}$ as

$$\sigma_z^{(p)\beta} = \left[1 + \frac{S_{32}^{(1)} S_{53}^{(1)}}{\tilde{S}_{52}^{(1)} S_{33}^{(1)}}\right] A_3^{(1)} + \left[\frac{S_{32}^{(1)} \tilde{\alpha}_5^{(1)}}{\tilde{S}_{52}^{(1)}} - \alpha_3^{(1)}\right] \frac{\Delta T}{S_{33}^{(1)}}. \tag{51}$$

Hence, the following relationship for A_3 may be established:

$$\iint_B \sigma_z^{(p)}\, dx\, dy = 4\left[1 + \frac{S_{32}^{(1)} S_{53}^{(1)}}{\tilde{S}_{52}^{(1)} S_{33}^{(1)}}\right] b(h_1 + h_2)\, A_3^{(1)} + 4\left[\frac{S_{32}^{(1)} \tilde{\alpha}_5^{(1)}}{\tilde{S}_{52}^{(1)}} - \alpha_3^{(1)}\right] b(h_1 + h_2)\, \frac{\Delta T}{S_{33}^{(1)}} \tag{52}$$

The contribution from the homogeneous solution may be obtained from Eqs. 28 and 39a by

$$\iint_B \sigma_z^{(h)}\, dx\, dy = \sum_m d_m\, \gamma_{3m}, \tag{53}$$

where

$$\gamma_{3m} = \iint_B f_{3m}(x,y;\, \delta_m)\, dx\, dy. \tag{54}$$

Substituting Eqs. 52 and 53 into Eqs. 19 and solving the resulting equation for A_3 in terms of d_m give

$$A_3^{(1)} = e_o + \sum_m d_m\, e_{3m}, \tag{55}$$

where e_{3m} are known constants obtained by integrating associated eigenfunctions, and e_o, from the particular solution.

The boundary conditions on $(\partial B - \partial B_F)$ suggest, by using Eqs. 28, 38, 43, 44, 49 and 50, the following relationships for determining the constants d_m:

$$\sum_m d_m f_{2m}^{(1)}(x,h_1;\ \delta_m) = \frac{S_{53}^{(1)}}{\tilde{S}_{52}^{(1)}} A_3^{(1)} + \frac{\tilde{\alpha}_5^{(1)}}{\tilde{S}_{52}^{(1)}} \Delta T, \tag{56a}$$

$$\sum_m d_m f_{4m}^{(1)}(x,h_1;\ \delta_m) = 0, \tag{56b}$$

$$\sum_m d_m f_{6m}^{(1)}(x,h_1;\ \delta_m) = 0, \tag{56c}$$

$$\sum_m d_m h_{1m}^{(2)}(x,-h_2;\delta_m) = 0, \tag{56d}$$

$$\sum_m d_m h_{2m}^{(2)}(x,-h_2,\delta_m) = 0, \tag{56e}$$

$$\sum_m d_m h_{3m}^{(2)}(x,-h_2;\delta_m) = 0, \tag{56f}$$

and

$$\sum_m d_m h_{1m}^{(\beta)}(b,y;\ \delta_m) = 0, \tag{56g}$$

$$\sum_m d_m h_{2m}^{(\beta)}(b,y;\ \delta_m) = 0, \qquad (\beta = 1,2) \tag{56h}$$

$$\sum_m d_m h_{3m}^{(\beta)}(b,y;\ \delta_m) = 0, \tag{56i}$$

where h_{ij} denote differentiated forms of g_{ij} according to Eqs. 43 and 44 with the origin of the Cartesian coordinates being transferred to the left free edge (Fig. 2). The boundary conditions shown in Eqs. 56a-i are matched by a boundary collocation method, using the eigenfunctions in Eq. 28. The constants d_m are then evaluated by satisfying these conditions at a given number of selected collocation stations. Accuracy and convergence of solutions and effects of collocation points along the boundaries are

reported elsewhere [9]. For the numerical results reported in this paper, 63 terms in the eigenfunction series and 74 collocation stations along the boundaries were used to ensure the accuracy and convergence of the solutions [9].

In what follows, laminate thermoelasticity solutions determined from the current eigenfunction expansion method are presented first and compared with existing approximate numerical solutions available in the literature. Detailed results characterizing the thermal boundary-layer field in the symmetric angle-ply composites with various lamination variables are given also.

4.2 *Thermal Boundary-Layer Stress Distribution*

Distributions of the in-plane and interlaminar thermal stresses, σ_z, τ_{xz}, σ_y and τ_{yz}, along the ply interface of a [45°/-45°/-45°/45°] graphite-epoxy laminate are shown in a semi-logarithmic plot in Fig. 3. Dotted lines in the figure represent the result given in [3] by using constant-strain triangular elements (CST) in a finite-element procedure. Solid lines denote the present laminate thermoelasticity solution with free-edge stress singularity being included. The two solutions are in good agreement in the region away from the laminate boundary. The in-plane stresses, σ_z and τ_{xz}, in the region away from the edge are found to be relatively constant and to recover to more or less what classical lamination theory (CLT) predicts. (Based on the classical lamination theory, the only stress induced by a unit change of temperature in the $[\pm 45]_s$ graphite-epoxy composite is a constant in-plane shear stress $\tau^{\circ}_{xz} = 28.8$ psi/°F.) As the edge is approached, the difference becomes gradually appreciable due to the presence of the stress singularity, which was not included in the previous approximate numerical solution. As

will be shown later, within the boundary-layer region the stress field is completely governed by the singular terms in the stress solution, and the interlaminar stress increases very rapidly. In fact, the interlaminar stress is much higher than the in-plane stress component as the edge of the laminate is infinitesmally approached. Thus thermally-induced deformation and failure may be dominated by the interlaminar stresses.

4.3 *Stress Singularity in Thermal Boundary-Layer Field*

Since the stress and strain fields within the boundary-layer region are governed by the singular terms in the present laminate thermoelasticity solution, theoretically, the thermally induced stresses determined from the solution are unbounded at the intersection of the ply interface and the laminate edge. Thus the near-field stress may be expressed in a general form as

$$\sigma_i = \sum_{k=1}^{3} \left(D_{ik} Z_k^{\delta_1} + D_{i(k+3)} \bar{Z}_k^{\delta_1} \right) + O(\text{higher-order, non-singular terms})$$

$$(i=1,2,3,\ldots,6) , \qquad (57)$$

where Z and $\bar{Z}$ have their origin at the intersection of the ply interface and the edge of the laminate (Fig. 2); δ_1 is the order of the thermal boundary-layer stress singularity which is the smallest eigenvalue satisfying

$$0 > \mathrm{Re}[\delta_1] > -1 \qquad (58)$$

among all the δ_m determined from the characteristic equation [9] in solving for the homogeneous solution of the governing partial differential equations. The order of the boundary-layer stress singularity is noted [9] to depend only upon lamina constitutive properties and fiber orientations of the adjacent plies. Numerical results of the first four nonzero eigenvalues δ_m for symmetric angle-ply $[\theta/-\theta/-\theta/\theta]$ graphite-epoxy laminates are given in Table 1.

Note that δ_1 corresponds to the order of boundary-layer stress singularity and that zero and intergers, n, are always eigenvalues for the problem. In this composite system, δ_1 has a value which is rather weak as compared with other typical singular stress problems such as an elastic crack problem. Among various θ studied, it appears that the $[\pm 51^\circ]_s$ graphite-epoxy laminate has the strongest stress singularity [9].

4.4 *Thermal Boundary-Layer Stress Intensity Factors*

For a composite laminate with given fiber orientations, the coefficients of the singular terms in Eq. 57 characterize amplitudes of the thermal stress and strain in the boundary-layer region. Because the boundary-layer stresses are most crucial along the ply interface, i.e., the x-axis, and become singular at the interface/edge intersection, it is possible to define the amplitudes of the singular thermal boundary-layer stresses by

$$K_i = \lim_{x \to 0} x^{-\delta_1} \sigma_i \qquad (i=1,2,3,\ldots,6). \tag{59}$$

The K_i are dependent upon geometric variables of the composite (e.g., ply thickness, number of layers), lamination parameters (e.g., fiber orientation, stacking sequence), and mechanical and thermal loading conditions. The fundamental structure of the thermal boundary-layer stress solution shown in Eqs. 57 and 59 resembles that of an elastic crack problem (except that δ_1 has a value of -0.5 in the crack-tip stress field). Also, the nature of K_i is similar to the so-called crack-tip stress intensity factors in linear elastic fracture mechanics. Thus, in this context, it may be appropriate to denote K_i as "thermal boundary-layer stress intensity factors" or "thermal free-edge stress intensity factors" for the composite laminate. Values of K_i for the $[\theta/-\theta/-\theta/\theta]$ graphite-epoxy composite with all laminae being of

equal thicknesses under unit thermal loading are determined in Table 2, in which K_i carry the unit of $[\text{psi-in.}]^{-\delta_1}$.

The K_i associated with the interlaminar stresses are found, in general, significantly larger than those associated with the in-plane stress components. The dominance of the interlaminar thermal stresses σ_y and τ_{yz} in the boundary-layer region shown in Fig. 3 is clearly illustrated by the high values of K_2 and K_4, which are, in fact, one or two orders of magnitude higher than the K_i associated with σ_x, σ_z and τ_{xz} for all θ studied. The high negative value of K_2 indicates that a large compressive interlaminar normal stress σ_y is developed near the edge. Note that K_6 is found to vanish for all angle-ply $[\pm\theta]_s$ composite laminates, due to the symmetry of ply orientations and traction-free edge conditions.

4.5 *Through-Thickness Distribution of Thermal Boundary-Layer Stresses*

The unique features of the thermal boundary-layer effect are further illustrated by through-the-thickness distributions of in-plane and interlaminar thermal stresses near the laminate boundary. The in-plane thermal stress σ_z in the thickness direction at different distances away from the edge are shown in Fig. 4. The current solution is in agreement with previous results [3] that σ_z is compressive in the most part of the section near the laminate boundary except for the region closest to the ply interface where boundary-layer stress singularity dominates. Through-the-thickness distributions of the most dominant thermal interlaminar stress τ_{yz} are given in Fig. 5. The gradient of τ_{yz} in the y-direction increases rapidly as the laminate edge is approached. Again the laminate elasticity solution in the boundary-layer region differs from the approximate solution [3] near the interface but in in good agreement in the far field. The next two figures (Figs. 6 and 7)

provide information on through-the-thickness distributions of thermal interlaminar shear and normal stresses, τ_{xy} and σ_y, in the [45°/-45°/-45°/45°] graphite-epoxy laminate. The τ_{xy} is found to change significantly with the thickness coordinate, alters its sign across the interface, and reaches a maximum value at a small distance y away from the interface. Within the boundary-layer region, τ_{xy} becomes very small along the interface and vanishes identically at the laminate boundary as envidenced by $K_6 = 0$. The distribution of σ_y at several distances near the boundary of the laminate is shown in Fig. 7. At any given x/b, σ_y is generally very small at a distance y away from the interface, and reaches a higher level as the interface y = h is approached. As one moves towards the edge, the interlaminar normal stress becomes very significant in compression. As $x \to 0$ and $y \to h$ the stress solution becomes unbounded due to the stress singularity at the intersection point.

4.6 *Thermal Boundary-Layer Width*

The rapid increase of thermal stress has been observed to be restricted to within a very localized region near the edge of the laminate--the so-called "thermal boundary-layer width." The thermal stresses developed in the boundary-layer region are inherently three-dimensional and cannot be determined by classical lamination theory. The singular nature and the extent of perturbation of the thermal boundary stress are considered to be of vital importance in controlling initiation of interlaminar fracture (or delamination) and strength degradation. The extent of perturbation of the laminate thermal stress field can be characterized by the boundary-layer width (or thickness), B. Pipes, et al. [10] defined the boundary-layer thickness as the distance from the edge, at which the interlaminar stress τ_{yz} is about 3 per cent of

the value calculated at the intersection of the ply interface and the edge of the laminate. The validity of this definition is somewhat questionable because the interlaminar stresses are singular at this point. In this study an alternative definition of the boundary-layer width is proposed on the basis of the strain energy density distribution in the composite laminate.

The strain energy density distributions E(x,y) along the interface of the [θ/-θ/-θ/θ] graphite-epoxy laminates are shown in Fig. 8. The strain energy density remains relatively constant in the far field where classical lamination theory holds, and increases drastically by an order of magnitude as the edge is approached. In this paper, the boundary-layer width B in a composite laminate is defined as the distance away from the edge where the strain energy density along the interface is three per cent higher than the nominal value E_o obtained in the far field. In general, $E(B,h^+)$ differs slightly from $E(B,h^-)$ due to the discontinuous in-plane stress components at $y = h^+$ and h^-; thus, an average value of B is designated as the width of the boundary-layer region. Based on this definition, values of B/W for [θ/-θ/-θ/θ] graphite-epoxy laminates are evaluated and shown in Fig. 9 It is obvious from the figure that the [45°/-45°/-45°/45°] graphite-epoxy laminate has a higher value of B/W than those composites with other fiber orientations. As θ changes towards either direction, B/W decreases rapidly. When θ has an angle of [±0°] or [±90°], B/W vanishes identically indicating that there is no boundary-layer effect in these cases since the two adjacent plies are identical.

4.7 *Effects of Fiber Orientation*

Effects of fiber orientation on the thermal boundary-layer response in [θ/-θ/-θ/θ] graphite-epoxy laminates are best illustrated by boundary-layer

thermal stresses along $\theta/-\theta$ ply interface. The thermal stresses are observed to be significantly affected by the alternation of fiber orientation. Figures 10 and 11 depict the distributions of thermal interlaminar shear stresses, τ_{xy} and τ_{yz}, along y = h. The τ_{xy} is relatively small for all fiber orientations studied, and the change of fiber orientation only alters the amplitude of the interlaminar shear stress slightly. The τ_{xy} reaches its maximum before it vanishes at the laminate boundary, where traction-free boundary conditions are satisfied exactly. The other thermal interlaminar shear component τ_{yz} is more significant in the boundary-layer region than τ_{xy}. The τ_{yz} has a higher value along the interface of the [45°/-45°/-45°/45°] graphite-epoxy laminate than those in other ply ocnfigurations due to the higher value of δ_1. As is expected, the interlaminar shear stress becomes unbounded as the laminate boundary is approached due to the stress singularity. As θ moves towards either side, the amplitude of the interlaminar shear stress decreases. The distribution of interlaminar normal stress σ_y along the interface of angle-ply laminates with different θ is shown in Fig. 12. The σ_y is found to be vanishingly small in the far field. It is small in tension first, then changes its sign, and becomes compressive as the free edge is approached. Like the interlaminar shear stress, σ_y becomes unbounded at the free edge (i.e., at x = b and y = h) and is significantly only within the boundary-layer region. In Fig. 13, distributions of in-plane thermal stress σ_z in $[\theta/-\theta/-\theta/\theta]$ graphite-epoxy are given. The laminate thermoelasticity solution reveals that σ_z has a very small value in the far field, and remains relatively constant before rapid increase in its magnitude, as the laminate boundary is approached. This is apparently different from the prediction of classical lamination theory, which suggests that, in the symmetric angle-ply $[\theta/-\theta/-\theta/\theta]$ composite laminate, the in-plane thermal stress σ_z vanishes

throughout the composite. At the intersection of the free edge and ply interface, again σ_z has an unbounded value due to the stress singularity at that point. In the boundary-layer region, σ_z along the interface in the $[\pm 45]_s$ laminate is found to have a higher value than in the composites with other ply configurations. As θ changes from 45°, the magnitude of σ_z decreases appreciably. In fact, the results shown in Fig. 13 indicate that σ_z becomes negligibly small for the cases with $\theta > 75°$.

4.8 *Effects of Relative Ply Thickness*

Another important laminate variable investigated in this study is the effect of ply thickness or volume of the layer that is stressed interlaminarly, since transverse deformation and failure in composites are affected significantly by lateral constraints in the laminates. It has been found that deformation and fracture in certain composite systems change significantly with the ply thickness while stacking sequence remains the same. In this paper, influences of ply thickness on the thermal boundary-layer stress in [45°/-45°/-45°/45°] graphite-epoxy laminate with various h_1/W are examined (W being kept constant). Following the aforementioned analytical procedure and solution scheme, a parametric study on thermal boundary-layer response in the composite laminates with various ply thicknesses h_1/W has been conducted. Numerical results showing the effect of h_1/W on thermal boundary-layer stress intensity factors are given in Table 3. The results indicate that, for a given laminate configuration and fiber orientation, the change of h_1/W does not alter the thermal stress singularity but does affect thermal boundary-layer stress intensity factors appreciably. The composite laminate with $h_1/W \simeq 0.4 \sim 0.5$, seems to have smaller values of K_i than other cases studied.

As h_1/W approaches 0 or 1, the boundary-layer stress intensity factors reach their maxima. The higher values of K_i developed in the composite by changing ply thickness h_1/W provide an important basis for evaluation of initiation of transverse cracking and interply delamination in composite laminates.

5. SUMMARY AND CONCLUSIONS

A study of thermal boundary-layer stresses in composite laminates has been presented. Formulation of the problem is based on the theory of anisotropic laminate thermoelasticity. With the aid of Lekhnitskii's complex-variable stress functions, an eigenfunction expansion method is used to establish a system of coupled, governing partial differential equations for the problem. Numerical results for symmetric angle-ply $[\theta/-\theta/-\theta/\theta]$ graphite-epoxy laminates are obtained. Effects of lamination and geometric variables on the thermal boundary-layer stress singularity and distributions are studied. Based on the information discussed in the previous sections, the following conclusions may be reached:

1. Thermal stresses in the boundary-layer region of a composite laminate are inherently three dimensional in nature. They cannot be calculated by the classical lamination theory, but can be determined explicitly by the current approach.
2. The thermal stress field in the boundary-layer region is singular in general. By using an eigenfunction expansion method, one can determine the order of the boundary-layer stress singularity by solving the characteristic transcendental equation obtained from the homogeneous solution. The order of the boundary-layer stress singularity depends on anisotropic thermoelastic properties of adjacent plies in the composite.
3. The boundary-layer thermal stress field may be characterized by "thermal boundary-layer stress intensity factors" or "thermal free-edge stress intensity factors." The K_i are functions of anisotropic thermoelastic constants of laminae, ply orientation

and laminate geometry, and may be used to evaluate strength degradation and initiation of interlaminar fracture (delamination) and transverse cracking. Their values can be determined by various methods such as the boundary collocation method and the finite element method.

4. Thermal boundary-layer thickness which characterizes the domain where classical lamination theory does not hold can be determined explicitly by considering the change of strain energy density along the ply interface. The thermal boundary-layer thickness depends on lamination variables, geometric parameters, thermal loading conditions and thermoelastic ply properties. In $[\pm\theta]_s$ graphite-epoxy composites, the case of $\theta = 45°$ possesses a higher thermal boundary-layer thickness than those of other fiber orientations studied.
5. In comparison with previous approximate solutions, good agreement in the far field is observed, but appreciable discrepancy near the laminate boundary occurs. The difference is attributed to the fact that, in the boundary-layer region, the thermoelastic solution is completely governed by the singular terms which previous approximate solutions failed to include.
6. The current method of approach is also valid for asymmetric composite laminates, since the bending, twisting and rotational components of deformation are included in the formulation.

6. ACKNOWLEDGMENTS

The work described in this paper was supported in part by the National Aeronautics and Space Administration-Lewis Research Center (NASA-LRC), Cleveland, Ohio under Grant NSG 3044. The authors are grateful to Dr. C. C. Chamis of NASA-LRC, Dr. G. P. Sendeckyj of the Air Force Flight Dynamics Laboratory, and Professor H. T. Corten of the University of Illinois at Urbana-Champaign for the valuable discussion and encouragement during the course of this study.

7. REFERENCES

1 Herakovich, C. T., "On Thermal Edge Effects in Composite Laminates," *International Journal of Mechanical Sciences*, Vol. 18, No. 3, 1976, pp. 129-134.

2 Herakovich, C. T., Renieri, G. D. and Brinson, H. F., "Finite Element Analysis of Mechanical and Thermal Edge Effects in Composite Laminates," *Proceedings of the Army Symposium on Solid Mechanics-Composite Materials: The Influence of Mechanics of Failure on Design*, AMMRC Report MS-76-2, Cape Cod, Mass., Sept. 1976, pp. 237-247.

3 Wang, A. S. D. and Cross, F. W., "Edge Effects on Thermally Induced Stresses in Composite Laminates," *Journal of Composite Materials*, Vol. 11, 1977, pp. 300-312.

4 Farley, G. L. and Herakovich, C. T., "Influence of Two-Dimensional Hygrothermal Gradients on Interlaminar Stresses Near Free Edges," *Advanced Composite Materials-Environmental Effects*, ASTM STP 568, J. R. Vinson, Ed., American Society for Testing and Materials, 1978, pp. 143-159.

5 Jones, R. M., *Mechanics of Composite Materials*, Scripta Book Co., Washington, D. C., 1975.

6 Pipes, R. B., Vinson, J. R. and Chou , T. W., "On the Hygrothermal Response of Laminate Composite Systems," *Journal of Composite Materials*, Vol. 10, 1976, pp. 129-148.

7 Lekhnitskii, S. G., *Theory of Elasticity of an Anisotropic Body*, Holden-Day, 1963.

8 Theocaris, P. S., "The Order of Singularity at a Multi-Wedge Corner of a Composite Plate," *International Journal of Engineering Science*, Vol. 12, 1974, pp. 107-120.

9 Wang, S. S. and Choi, I., "Boundary-Layer Effects in Composite Laminates; Part I--Free-Edge Stress Singularity; Part II--Free-Edge Stress Distributions and Basic Characteristics," to appear in *Journal of Applied Mechanics*, Trans. ASME, 1982.

10 Pipes, R. B. and Pagano, N.S., "Interlaminar Stresses in Composite Laminates under Uniform Axial Extension," *Journal of Composite Materials*, Vol. 4, 1970, pp. 538-548.

Table 1

First four nonzero eigenvalues for thermal boundary-layer stresses in symmetric angle-ply [θ/-θ/-θ/θ] graphite-epoxy laminates*

θ°	δ_1	$\delta_{2,3}$	δ_4
15°	-0.64322 E-3	0.99670 ± 0.04191 i	1.
30°	-0.11658 E-1	0.95521 ± 0.15271 i	1.
45°	-0.25575 E-1	0.88147 ± 0.23401 i	1.
60°	-0.23346 E-1	0.83074 ± 0.27138 i	1.
75°	-0.89444 E-2	0.86469 ± 0.25007 i	1.

*δ_1 corresponding to the strength of thermal boundary-layer stress singularity.

Table 2

Thermal boundary-layer stress intensity factors, K_i, along the interface of [θ/-θ/-θ/θ] graphite-epoxy composite laminates*†

θ	K_1	K_2	K_3	K_4	K_5	K_6
15°	4.5996 E-1	-3.8534 E 2	-3.7120 E 1	-5.2624 E 3	8.0636 E 0	0
30°	4.7031 E 0	-1.6466 E 2	8.6078 E 0	-5.7404 E 2	2.2357 E 1	0
45°	1.4546 E 1	-1.9130 E 2	-7.4958 E-1	-4.1747 E 2	3.6662 E 1	0
60°	1.3746 E 1	-1.7881 E 2	-2.2426 E 1	-3.7858 E 2	2.4394 E 1	0
75°	4.5752 E 0	-1.5101 E 2	-2.9205 E 1	-4.9611 E 2	8.5717 E 0	0

*$h_1 = h_2 = h$, $b = 8h$

†Values of K_i are per °F change

Table 3

Lamina thickness/volume effects on thermal boundary-layer stress intensity factors for [45°/-45°/-45°/45°] Graphite-Epoxy Laminates*†

h_1/W	K_1	K_2	K_3	K_4	K_5	K_6
0.2	1.4870 E 1	-1.9554 E 2	-7.6620 E-1	-4.2672 E 2	3.7475 E 1	0
0.4	1.4509 E 1	-1.9079 E 2	-7.4759 E-1	-4.1636 E 2	3.6565 E 1	0
0.5	1.4548 E 1	-1.9130 E 2	-7.4958 E-1	-4.1747 E 2	3.6662 E 1	0
0.6	1.4707 E 1	-1.9339 E 2	-7.5780 E-1	-4.2204 E 2	3.7064 E 1	0
0.8	1.5580 E 1	-2.0487 E 2	-8.0275 E-1	-4.4708 E 2	3.9263 E 1	0

*2b = 8W where W = constant = half laminate thickness

†Values of K_i are per °F change

8. LIST OF FIGURE CAPTIONS

Fig. 1 Coordinates and Geometry of Symmetric Angle-Ply $[\theta_1/\theta_2/\theta_2/\theta_1]$ Composite Laminate

Fig. 2 Free-Edge Geometry and Interface between k-th and (k+1)th Plies

Fig. 3 In-plane and Interlaminar Thermal Stresses along Interface in [45°/-45°/-45°/45°] Graphite-Epoxy Laminate, ($h_1=h_2=h$, $b=8h$)

Fig. 4 Through-Thickness Distribution of Boundary-Layer Thermal Stress σ_z in [45°/-45°/-45°/45°] Graphite-Epoxy Composite ($h_1=h_2=h$, $b=8h$)

Fig. 5 Through-Thickness Distribution of Boundary-Layer Thermal Stress τ_{yz} in [45°/-45°/-45°/45°] Graphite-Epoxy Composite

Fig. 6 Through-Thickness Distribution of Boundary-Layer Thermal Stress τ_{xy} in [45°/-45°/-45°/45°] Graphite-Epoxy Composite

Fig. 7 Through-Thickness Distribution of Boundary-Layer Thermal Stress σ_y in [45°/-45°/-45°/45°] Graphite-Epoxy Composite

Fig. 8 Strain Energy Density Distribution along Interface in [θ/-θ/-θ/θ] Graphite-Epoxy Composites ($h_1=h_2=h$, $b/W=6$)

Fig. 9 Thermal Boundary-Layer Thickness versus Ply Orientation in [θ/-θ/-θ/θ] Graphite-Epoxy Composites

Fig. 10 Thermal Interlaminar Shear Stress τ_{xy} along Interface in [θ/-θ/-θ/θ] Graphite-Epoxy Composites ($h_1=h_2=h$, $b=8h$)

Fig. 11 Thermal Interlaminar Shear Stress τ_{yz} along Interface in [θ/-θ/-θ/θ] Graphite-Epoxy Composites

Fig. 12 Thermal Interlaminar Normal Stress σ_y along Interface in [θ/-θ/-θ/θ] Graphite-Epoxy Composites

Fig. 13 In-plane Thermal Stress σ_z along Interface in [θ/-θ/-θ/θ] Graphite-Epoxy Composites

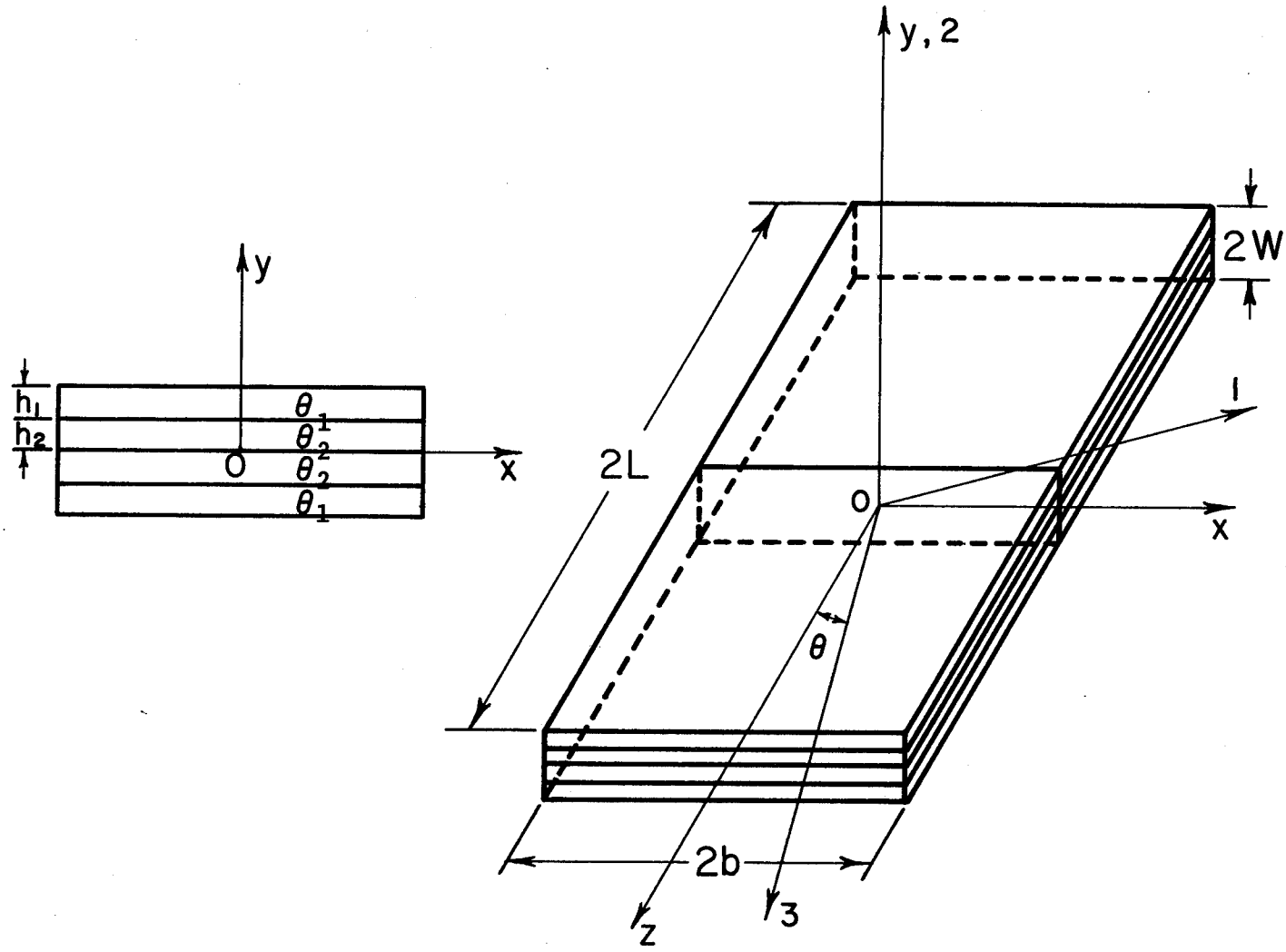

FIG. 1 COORDINATES AND GEOMETRY OF SYMMETRIC ANGLE-PLY $[\theta_1/\theta_2/\theta_2/\theta_1]$ COMPOSITE LAMINATE

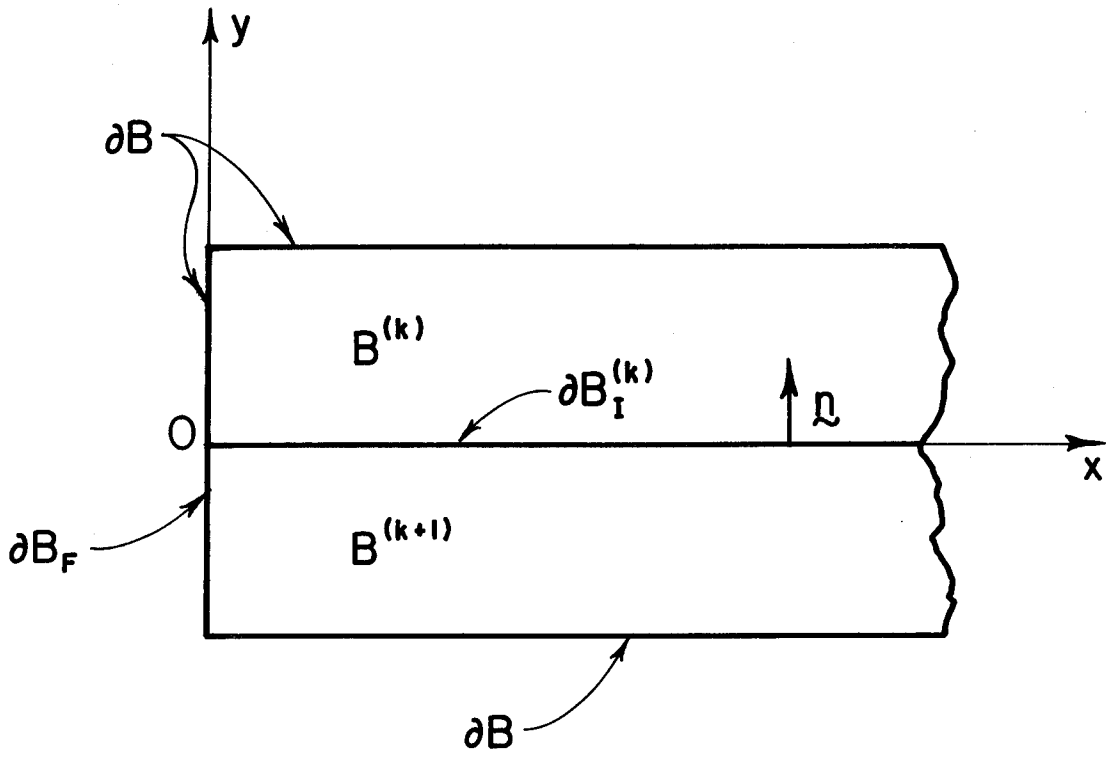

FIG. 2 FREE-EDGE GEOMETRY AND INTERFACE BETWEEN K-TH AND (K+1)TH PLIES

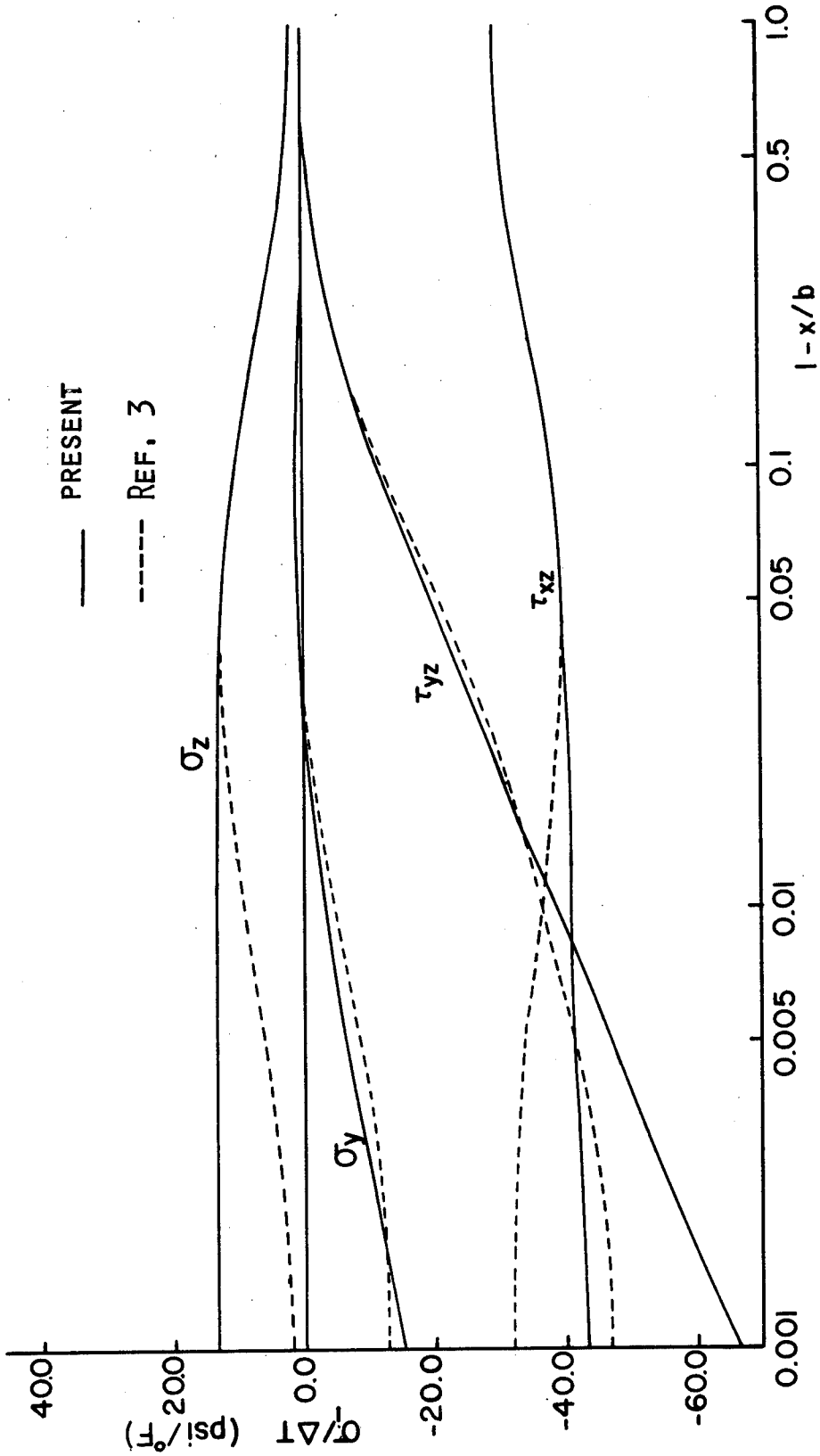

FIG. 3 IN-PLANE AND INTERLAMINAR THERMAL STRESSES ALONG INTERFACE IN [45°/-45°/-45°/45°] GRAPHITE-EPOXY LAMINATE, ($h_1 = h_2 = h$, $b = 8h$)

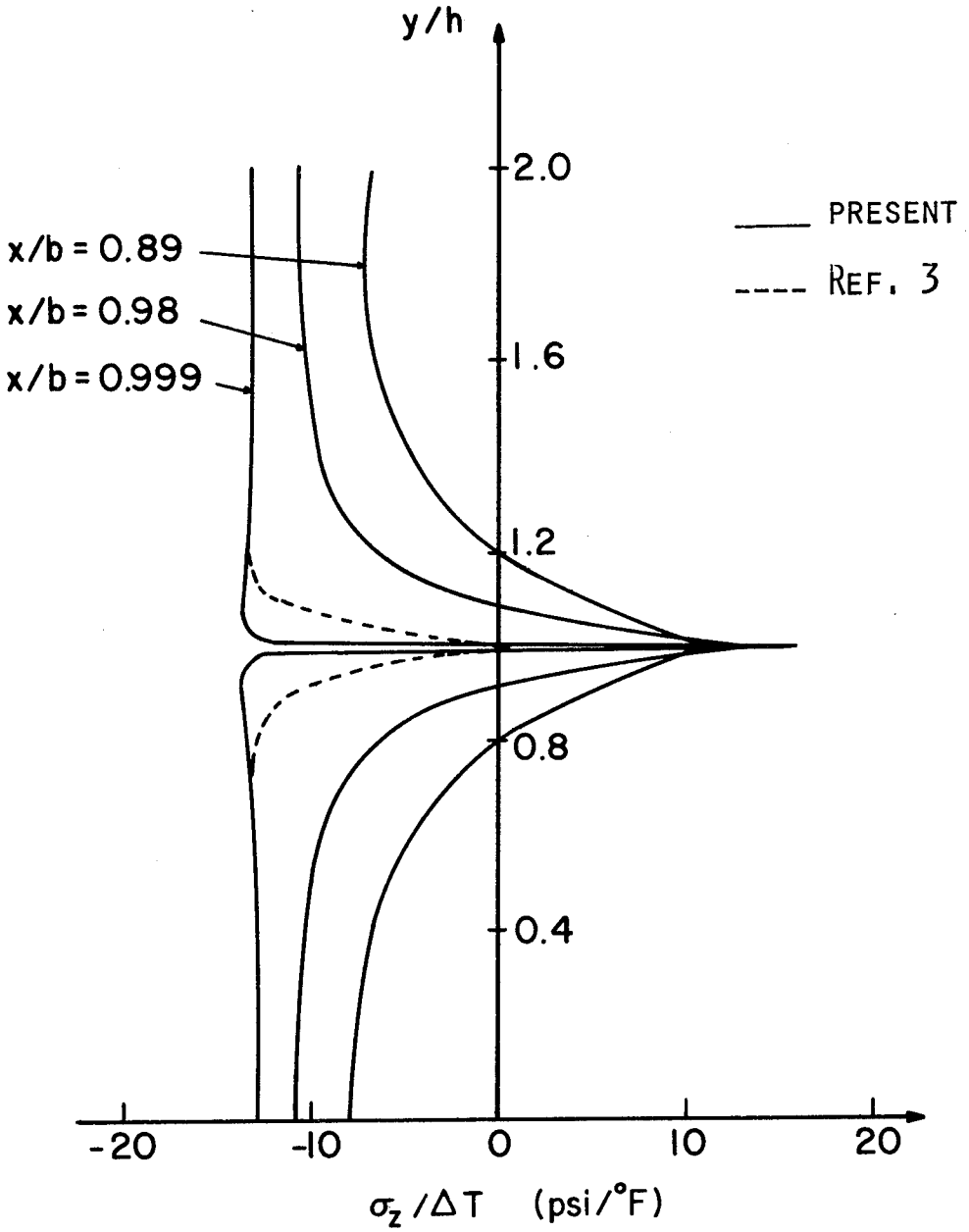

FIG. 4 THROUGH-THICKNESS DISTRIBUTION OF BOUNDARY-LAYER THERMAL STRESS σ_z IN [45°/-45°/-45°/45°] GRAPHITE-EPOXY COMPOSITE ($h_1 = h_2 = h$, $b = 8h$)

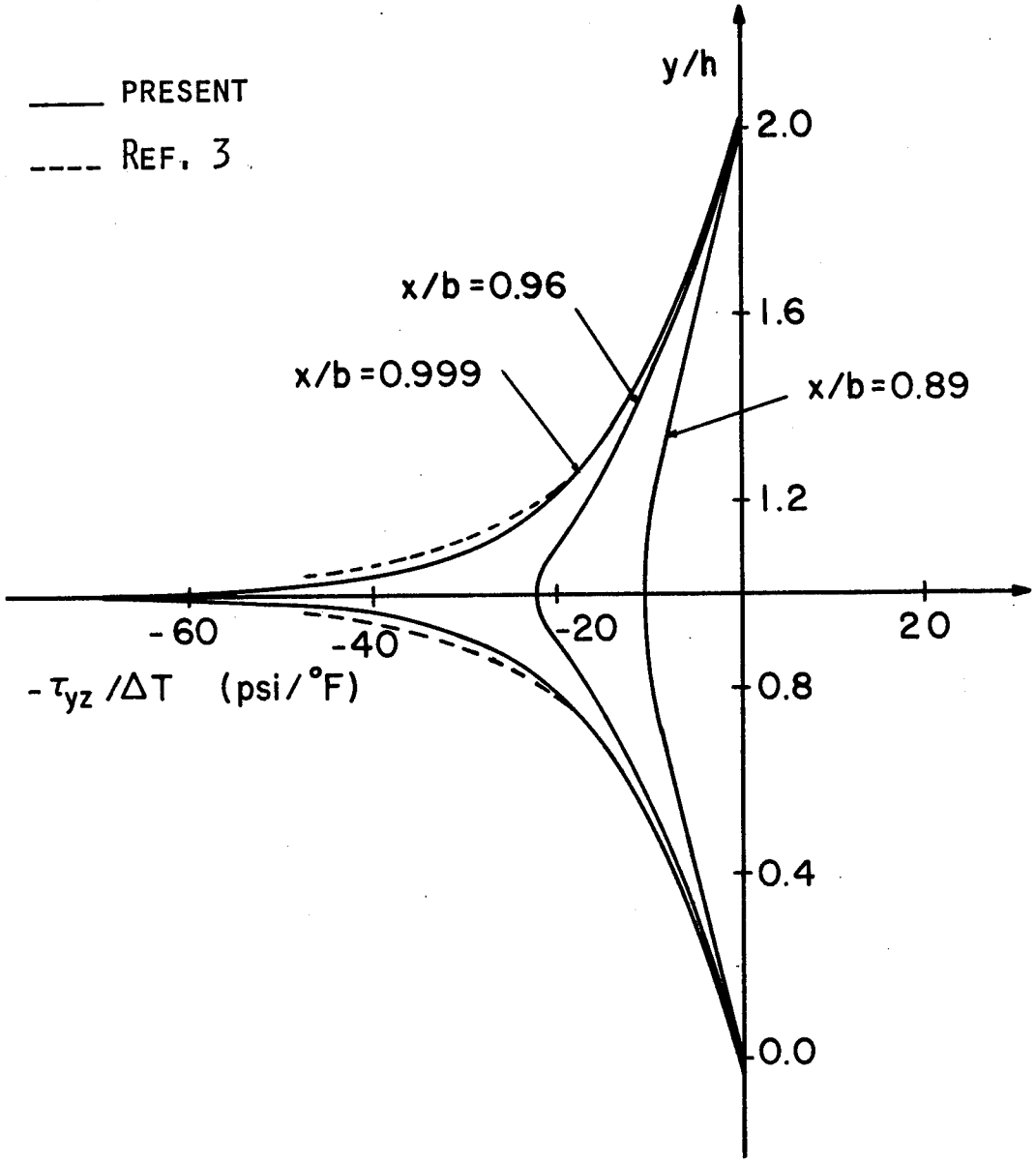

FIG. 5 THROUGH-THICKNESS DISTRIBUTION OF BOUNDARY-LAYER THERMAL STRESS τ_{yz} IN [45°/-45°/-45°/45°] GRAPHITE-EPOXY COMPOSITE

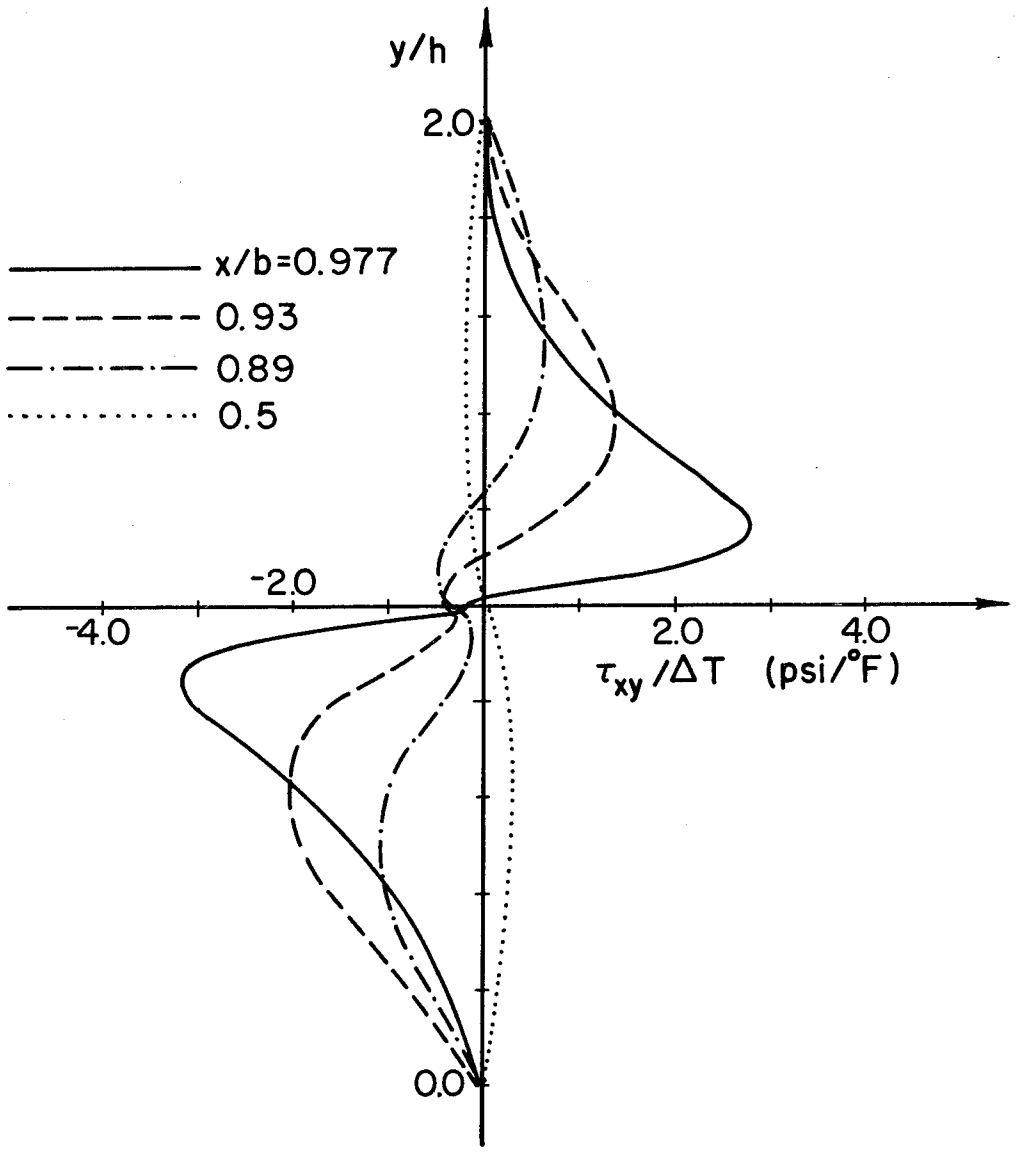

FIG. 6 THROUGH-THICKNESS DISTRIBUTION OF BOUNDARY-LAYER THERMAL STRESS τ_{xy} IN [45°/-45°/-45°/45°] GRAPHITE-EPOXY COMPOSITE

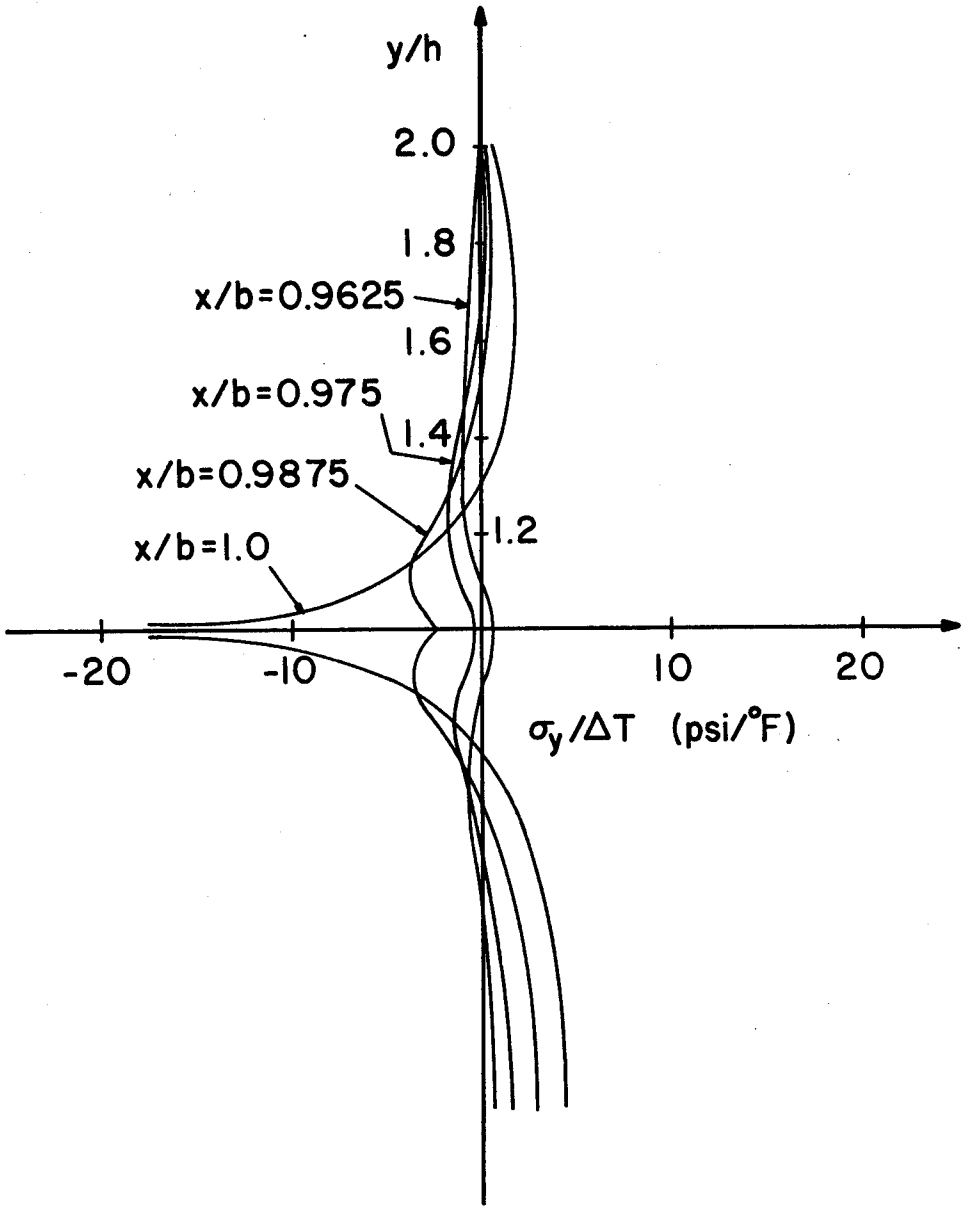

FIG. 7 THROUGH-THICKNESS DISTRIBUTION OF BOUNDARY-LAYER THERMAL STRESS σ_y IN [45°/-45°/-45°/45°] GRAPHITE-EPOXY COMPOSITE

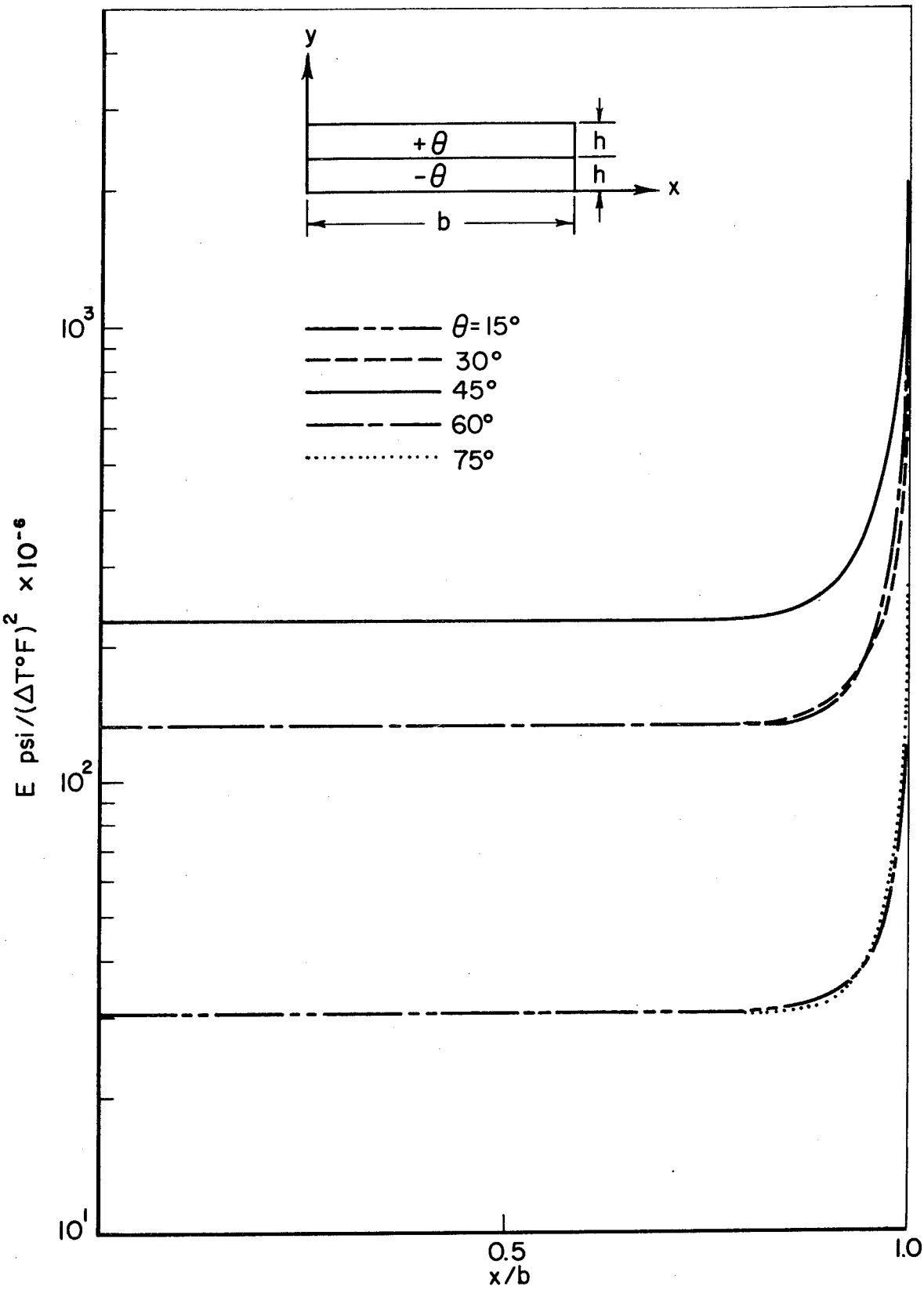

FIG. 8 STRAIN ENERGY DENSITY DISTRIBUTION ALONG INTERFACE IN [θ/-θ/-θ/θ] GRAPHITE-EPOXY COMPOSITES ($h_1 = h_2 = h$, $b/W = 6$)

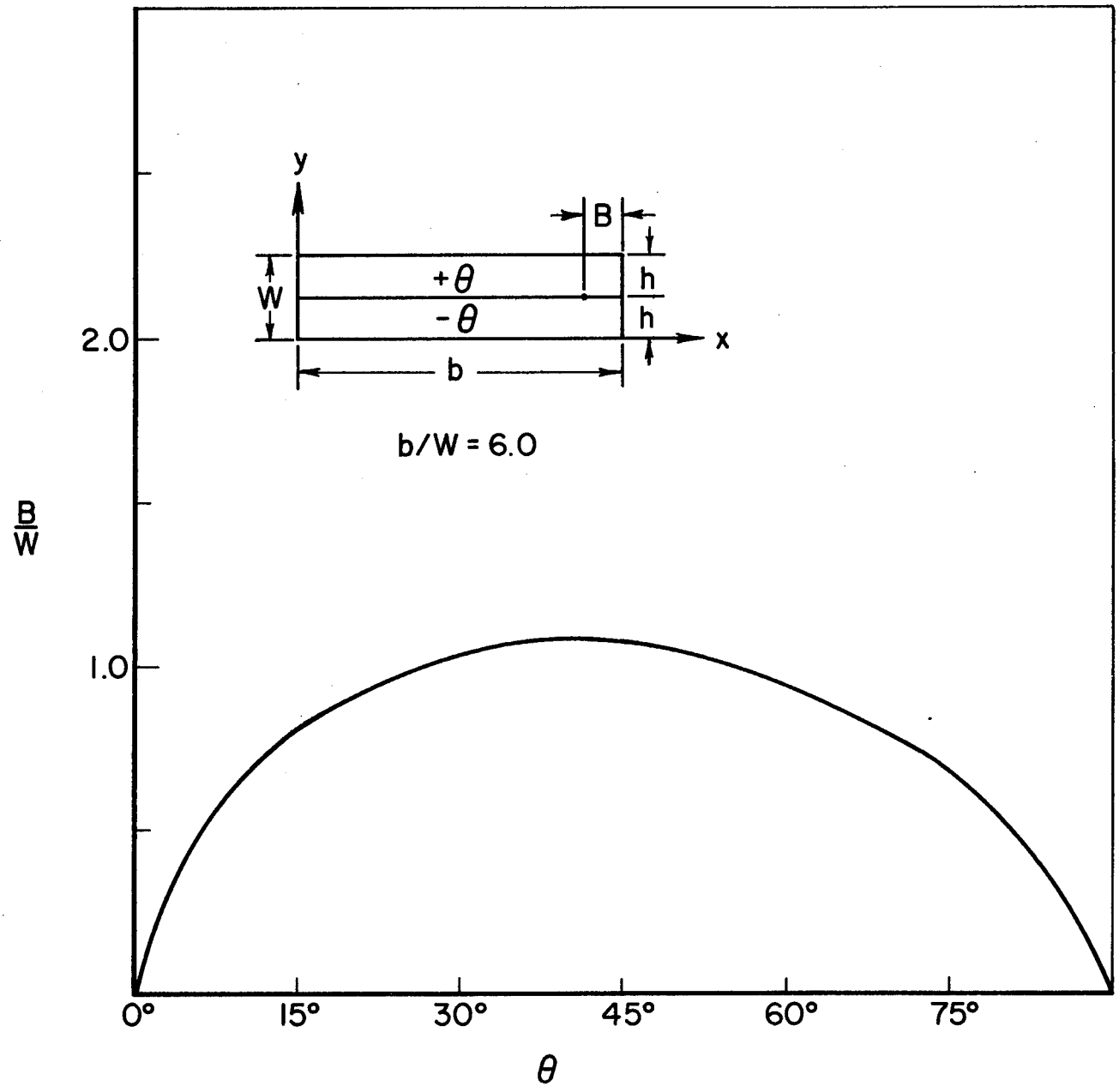

FIG. 9 THERMAL BOUNDARY-LAYER THICKNESS VERSUS PLY ORIENTATION IN [θ/-θ/-θ/θ] GRAPHITE-EPOXY COMPOSITES

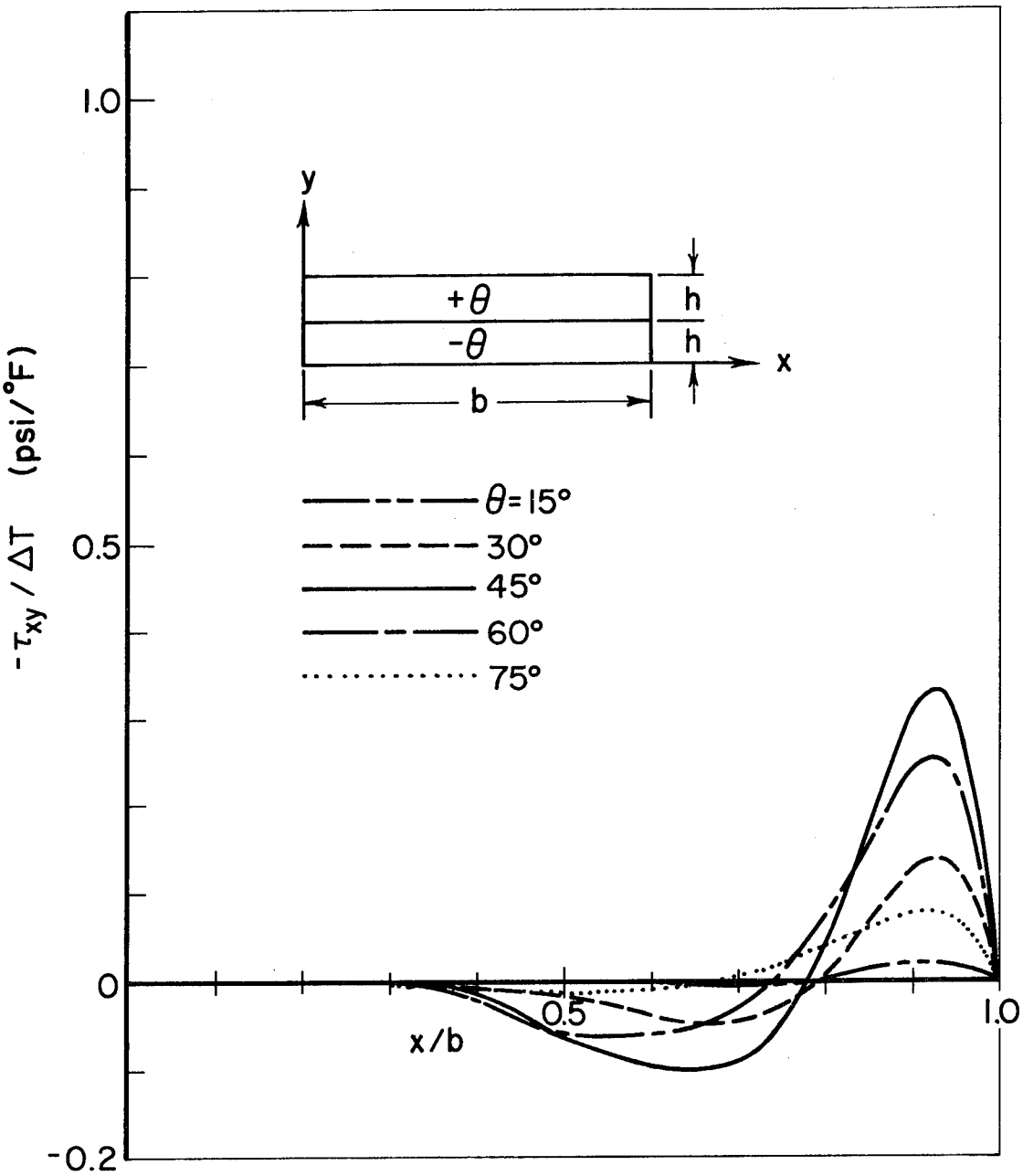

FIG. 10 THERMAL INTERLAMINAR SHEAR STRESS τ_{xy} ALONG INTERFACE IN [θ/-θ/-θ/θ] GRAPHITE-EPOXY COMPOSITES ($h_1 = h_2 = h$, $b = 8h$)

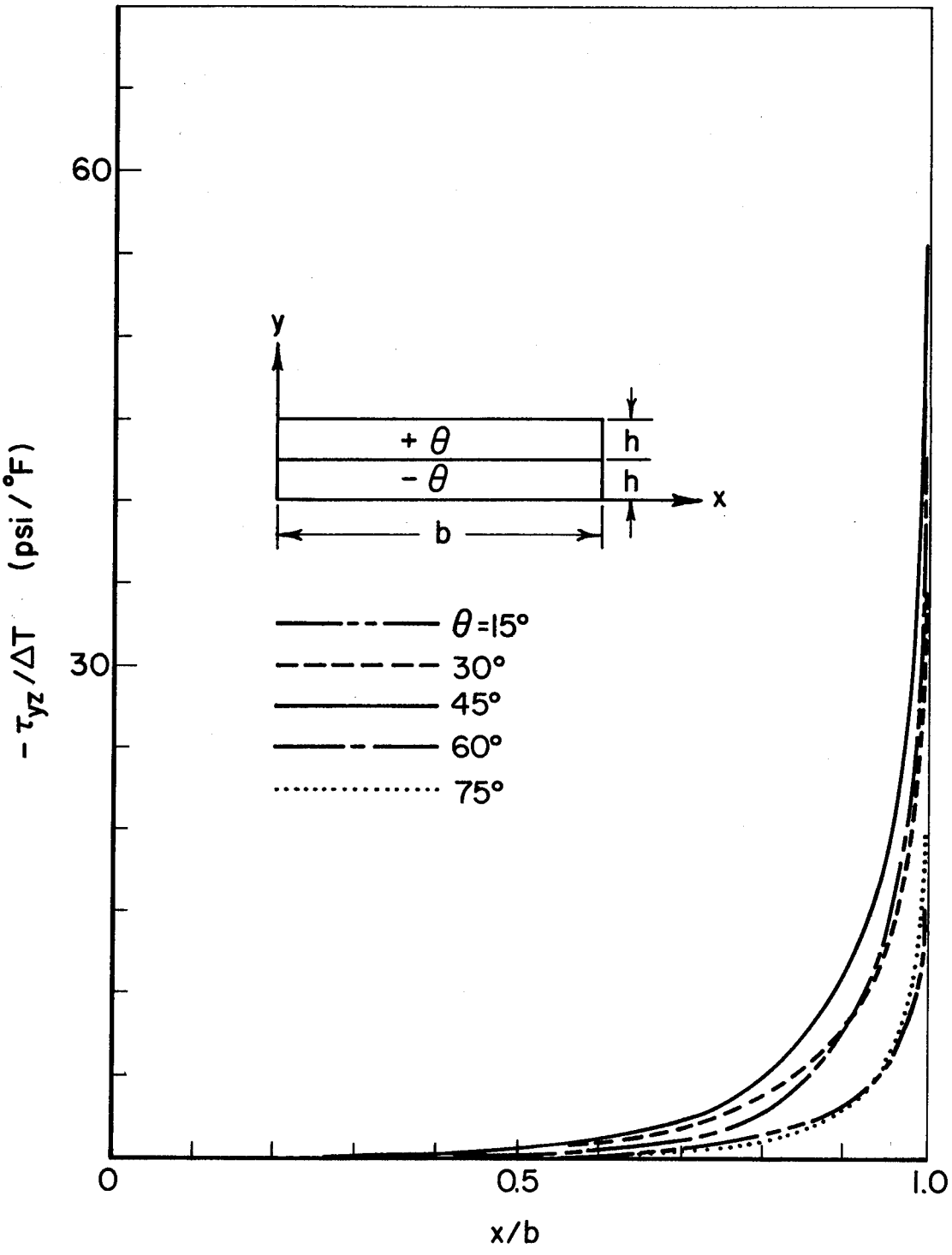

FIG. II THERMAL INTERLAMINAR SHEAR STRESS τ_{yz} ALONG INTERFACE IN [θ/-θ/-θ/θ] GRAPHITE-EPOXY COMPOSITES

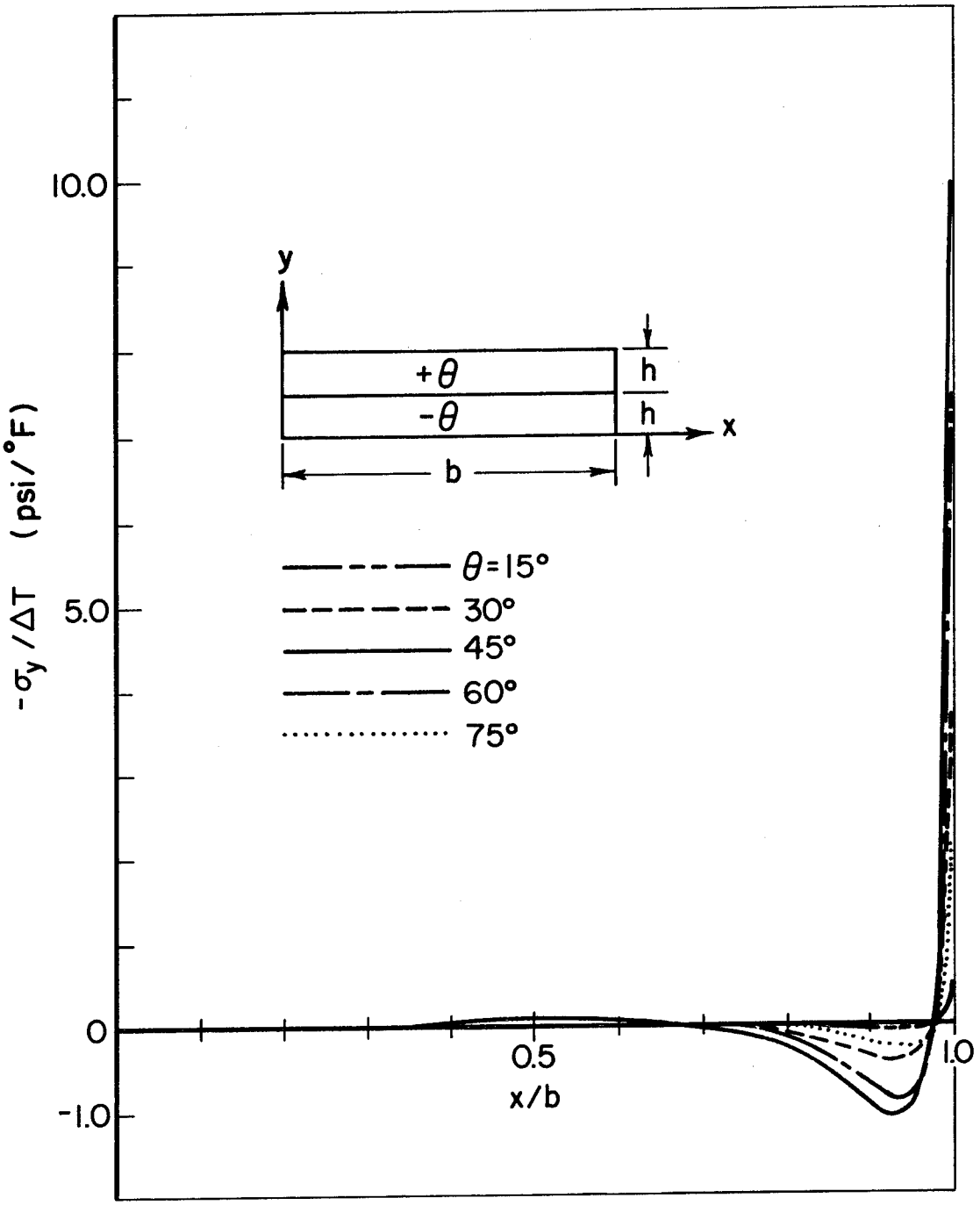

FIG. 12 THERMAL INTERLAMINAR NORMAL STRESS σ_y ALONG INTERFACE IN [θ/-θ/-θ/θ] GRAPHITE-EPOXY COMPOSITES

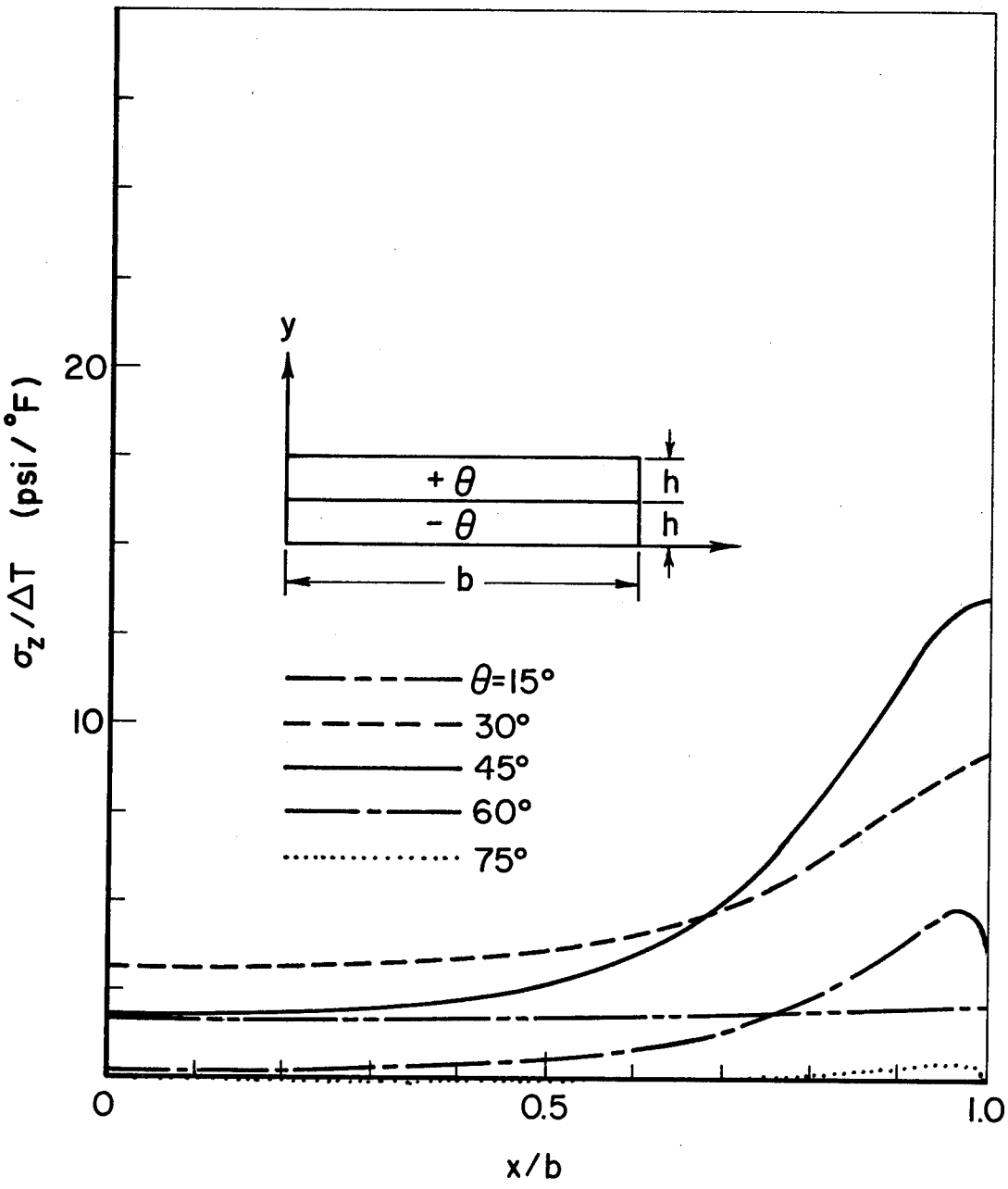

FIG. 13 IN-PLANE THERMAL STRESS σ_z ALONG INTERFACE IN [θ/-θ/-θ/θ] GRAPHITE-EPOXY COMPOSITES

FINAL REPORT - PART I - NSG3044

DISTRIBUTION LIST FOR NASA CR-165412

BOUNDARY LAYER THERMAL STRESSES IN ANGLE-PLY COMPOSITE LAMINATES

Advanced Research Projects Agency
Washington DC 20525
Attn: Library

Advanced Technology Center, Inc.
LTV Aerospace Corporation
P.O. Box 6144
Dallas, TX 75222
Attn: D. H. Petersen
W. J. Renton

Air Force Flight Dynamics Laboratory
Wright-Patterson Air Force Base, OH 45433
Attn: E. E. Baily
G. P. Sendeckyj (FBC)
R. S. Sandhu

Air Force Materials Laboratory
Wright-Patterson Air Force Base, OH 45433
Attn: H. S. Schwartz (LN)
T. J. Reinhart (MBC)
G. P. Peterson (LC)
E. J. Morrisey (LAE)
S. W. Tsai (MBM)
N. J. Pagano
J. M. Whitney (MBM)

Air Force Office of Scientific Research
Washington DC 20333
Attn: J. F. Masi (SREP)

Air Force Office of Scientific Research
1400 Wilson Blvd.
Arlington, VA 22209

AFOSR/NA
Bolling AFB, DC 20332
Attn: A. K. Amos

Air Force Rocket Propulsion Laboratory
Edwards, CA 93523
Attn: Library

Babcock & Wilcox Company
Advanced Composites Department
P.O. Box 419
Alliance, Ohio 44601
Attn: P. M. Leopold

Bell Helicopter Company
P.O. Box 482
Ft. Worth, TX 76101
Attn: H. Zinberg

The Boeing Company
P. O. Box 3999
Seattle, WA 98124
Attn: J. T. Hoggatt, MS. 88-33
T. R. Porter

The Boeing Company
Vertol Division
Morton, PA 19070
Attn: E. C. Durchlaub

Battelle Memorial Institute
Columbus Laboratories
505 King Avenue
Columbus, OH 43201
Attn: L. E. Hulbert

Bendix Advanced Technology Center
9140 Old Annapolis Rd/Md. 108
Columbia, MD 21045
Attn: O. Hayden Griffin

Brunswick Corporation
Defense Products Division
P. O. Box 4594
43000 Industrial Avenue
Lincoln, NE 68504
Attn: R. Morse

Celanese Research Company
86 Morris Ave.
Summit, NJ 07901
Attn: H. S. Kliger

Commander
Natick Laboratories
U. S. Army
Natick, MA 01762
Attn: Library

Commander
Naval Air Systems Command
U. S. Navy Department
Washington DC 20360
Attn: M. Stander, AIR-43032D

Commander
Naval Ordnance Systems Command
U.S. Navy Department
Washington DC 20360
Attn: B. Drimmer, ORD-033
M. Kinna, ORD-033A

Cornell University
Dept. Theoretical & Applied Mech.
Thurston Hall
Ithaca, NY 14853
Attn: S. L. Phoenix

Defense Metals Information Center
Battelle Memorial Institute
Columbus Laboratories
505 King Avenue
Columbus, OH 43201

Department of the Army
U.S. Army Aviation Materials Laboratory
Ft. Eustis, VA 23604
Attn: I. E. Figge, Sr.
Library

Department of the Army
U.S. Army Aviation Systems Command
P.O. Box 209
St. Louis, MO 63166
Attn: R. Vollmer, AMSAV-A-UE

Department of the Army
Plastics Technical Evaluation Center
Picatinny Arsenal
Dover, NJ 07801
Attn: H. E. Pebly, Jr.

Department of the Army
Watervliet Arsenal
Watervliet, NY 12189
Attn: G. D'Andrea

Department of the Army
Watertown Arsenal
Watertown, MA 02172
Attn: A. Thomas

Department of the Army
Redstone Arsenal
Huntsville, AL 35809
Attn: R. J. Thompson, AMSMI-RSS

Department of the Navy
Naval Ordnance Laboratory
White Oak
Silver Spring, MD 20910
Attn: R. Simon

Department of the Navy
U.S. Naval Ship R&D Laboratory
Annapolis, MD 21402
Attn: C. Hersner, Code 2724

Director
Deep Submergence Systems Project
6900 Wisconsin Avenue
Washington DC 20015
Attn: H. Bernstein, DSSP-221

Director
Naval Research Laboratory
Washington DC 20390
Attn: Code 8430
I. Wolock, Code 8433

Drexel University
32nd and Chestnut Streets
Philadelphia, PA 19104
Attn: P. C. Chou

E. I. DuPont DeNemours & Co.
DuPont Experimental Station
Wilmington, DE 19898
Attn: D. L. G. Sturgeon

Fiber Science, Inc.
245 East 157 Street
Gardena, CA 90248
Attn: E. Dunahoo

General Dynamics
P.O. Box 748
Ft. Worth, TX 76100
Attn: D. J. Wilkins
Library

General Dynamics/Convair
P.O. Box 1128
San Diego, CA 92112
Attn: J. L. Christian
R. Adsit

General Electric Co.
Evendale, OH 45215
Attn: C. Stotler
R. Ravenhall

General Motors Corporation
Detroit Diesel-Allison Division
Indianapolis, IN 46244
Attn: M. Herman

Georgia Institute of Technology
School of Aerospace Engineering
Atlanta, GA 30332
Attn: L. W. Rehfield

Grumman Aerospace Corporation
Bethpage, Long Island, NY 11714
Attn: S. Dastin
J. B. Whiteside

Hamilton Standard Division
United Aircraft Corporation
Windsor Locks, CT 06096
Attn: W. A. Percival

Hercules, Inc.
Allegheny Ballistics Laboratory
P. O. Box 210
Cumberland, MD 21053
Attn: A. A. Vicario

Hughes Aircraft Company
Culver City, CA 90230
Attn: A. Knoell

Illinois Institute of Technology
10 West 32 Street
Chicago, IL 60616
Attn: L. J. Broutman

IIT Research Institute
10 West 35 Street
Chicago, IL 60616
Attn: I. M. Daniel

Jet Propulsion Laboratory
4800 Oak Grove Drive
Pasadena, CA 91103
Attn: Library

Lawrence Livermore Laboratory
P.O. Box 808, L-421
Livermore, CA 94550
Attn: T. T. Chiao
E. M. Wu

Lehigh University
Institute of Fracture &
Solid Mechanics
Bethlehem, PA 18015
Attn: G. C. Sih

Lockheed-Georgia Co.
Advanced Composites Information Center
Dept. 72-14, Zone 402
Marietta, GA 30060
Attn: T. M. Hsu

Lockheed Missiles and Space Co.
P.O. Box 504
Sunnyvale, CA 94087
Attn: R. W. Fenn

Lockheed-California
Burbank, CA 91503
Attn: J. T. Ryder
K. N. Lauraitis
J. C. Ekvall

McDonnell Douglas Aircraft Corporation
P.O. Box 516
Lambert Field, MS 63166
Attn: J. C. Watson

McDonnell Douglas Aircraft Corporation
3855 Lakewood Blvd.
Long Beach, CA 90810
Attn: L. B. Greszczuk

Material Sciences Corporation
1777 Walton Road
Blue Bell, PA 19422
Attn: B. W. Rosen

Massachusetts Institute of Technology
Cambridge, MA 02139
Attn: F. J. McGarry
J. F. Mandell
J. W. Mar

NASA-Ames Research Center
Moffett Field, CA 94035
Attn: Dr. J. Parker
Library

NASA-Flight Research Center
P.O. Box 273
Edwards, CA 93523
Attn: Library

NASA-George C. Marshall Space Flight Center
Huntsville, AL 35812
Attn: C. E. Cataldo, S&E-ASTN-MX
Library

NASA-Goddard Space Flight Center
Greenbelt, MD 20771
Attn: Library

NASA-Langley Research Center
Hampton, VA 23365
Attn: J. H. Starnes
J. G. Davis, Jr.
M. C. Card
J. R. Davidson

NASA-Lewis Research Center
21000 Brookpark Road, Cleveland, OH 44135

Attn: Contracting Officer, MS ~~500-312~~ 501-11
Tech. Report Control, MS 5-5
Tech. Utilization, MS 3-16
AFSC Liaison, MS 501-3
S&MTD Contract Files, MS 49-6
L. Berke, MS 49-6
N. T. Saunders, MS 49-1
R. F. Lark, MS 49-6
J. A. Ziemianski, MS 49-6
R. H. Johns, MS 49-6
C. C. Chamis, MS 49-6 (8 copies)
R. L. Thompson, MS 49-6
T. T. Serafini, MS 49-1
Library, MS 60-3 (2 copies)

NASA-Lyndon B. Johnson Space Center
Houston, TX 77001
Attn: S. Glorioso, SMD-ES52
Library

NASA Scientific and Tech. Information Facility
P.O. Box 8757
Balt/Wash International Airport, MD 21240
Attn: Acquisitions Branch (15 copies)

National Aeronautics & SpaceAdministration
Office of Advanced Research & Technology
Washington DC 20546
Attn: L. Harris, Code RTM-6
M. Greenfield, Code RTM-6
D. J. Weidman, Code RTM-6

National Aeronautics & Space Administration
Office of Technology Utilization
Washington DC 20546

National Bureau of Standards
Eng. Mech. Section
Washington DC 20234
Attn: R. Mitchell

National Science Foundation
Engineering Division
1800 G. Street, NW
Washington DC 20540
Attn: Library

Northrop Corporation Aircraft Group
3901 West Broadway
Hawthorne, CA 90250
Attn: R. M. Verette
G. C. Grimes

Pratt & Whitney Aircraft
East Hartford, CT 06108
Attn: J. M. Woodward

Raytheon Co., Missile System Division
Mechanical Systems Laboratory
Bedford, MA
Attn: P. R. Digiovanni

Rensselaer Polytechnic Institute
Troy, NY 12181
Attn: R. Loewy

Rockwell International
Los Angeles Division
International Airport
Los Angles, CA 90009
Attn: L. M. Lackman
D. Y. Konishi

Sikorsky Aircraft Division
United Aircraft Corporation
Stratford, CT 06602
Attn: Library

Southern Methodist University
Dallas, TX 75275
Attn: R. M. Jones

Space & Missile Systems Organization
Air Force Unit Post Office
Los Angeles, CA 90045
Attn: Technical Data Center

Structural Composites Industries, Inc.
6344 N. Irwindale Avenue
Azusa, CA 91702
Attn: R. Gordon

Texas A&M
Mechanics & Materials Research Center
College Station, TX 77843
Attn: R. A. Schapery
Y. Weitsman

TRW, Inc.
23555 Euclid Avenue
Cleveland, OH 44117
Attn: I. J. Toth

Union Carbide Corporation
P. O. Box 6116
Cleveland, OH 44101
Attn: J. C. Bowman

United Technologies Research Center
East Hartford, CT 06108
Attn: R. C. Novak
Dr. A. Dennis

University of Dayton Research Institute
Dayton, OH 45409
Attn: R. W. Kim

University of Delaware
Mechanical & Aerospace Engineering
Newark, DE 19711
Attn: B. R. Pipes

University of Illinois
Department of Theoretical & Applied Mechanics
Urbana, IL 61801
Attn: S. S. Wang

University of Oklahoma
School of Aerospace Mechanical & Nuclear Engineering
Norman, OK 73069
Attn: C. W. Bert

University of Wyoming
College of Engineering
University Station Box 3295
Laramie, WY 82071
Attn: D. F. Adams

U. S. Army Materials & Mechanics Research Center
Watertown Arsenal
Watertown, MA 02172
Attn: E. M. Lenoe
D. W. Oplinger

V.P. I. and S. U.
Dept. of Eng. Mech.
Blacksburg, VA 24061
Attn: R. H. Heller
H. J. Brinson
C. T. Herakovich
K. L. Reifsnider